Spatiotemporal Variability of the Nitrogen Deficit in Bottom Waters on the Eastern Bering Sea Shelf

Calvin W. Mordy[1,2*], Lisa Eisner[3], Kelly Kearney[1,3], David Kimmel[3], Michael W. Lomas[4], Kathy Mier[3], Peter Proctor[1,2], Patrick H. Ressler[3], Phyllis Stabeno[2], and Eric Wisegarver[2]

[1]Cooperative Institute for Climate, Ocean, and Ecosystem Studies (CICOES), Box 355672, University of Washington, Seattle, WA 98105-5672, USA
mordy@uw.edu, Phone (206) 526-6870
proctor@uw.edu, Phone (206) 526-6217

[2]Pacific Marine Environmental Laboratory, NOAA, 7600 Sand Point Way, NE, Seattle WA 98115, USA
Phyllis.Stabeno@noaa.gov, Phone (206) 526-6453
Eric.Wisegarver@noaa.gov, Phone (206) 526-6762

[3]Alaska Fisheries Science Center, 7600 Sand Point Way NE, Seattle, WA 98115
Kathy.Mier@noaa.gov, Phone (206) 526-4276
Lisa.Eisner@noaa.gov, Phone (206) 526-4060
Kelly.Kearney@noaa.gov, Phone (206) 526-4617
David.Kimmel@noaa.gov, Phone (206) 526-4470
Patrick.Ressler@noaa.gov, Phone (206) 526-4785

[4]Bigelow Laboratory for Ocean Sciences, East Boothbay, ME 04544, USA
mlomas@bigelow.org, Phone +001 207 315 2567 ext. 311

*Corresponding Author

ABSTRACT

As water flows from the North Pacific Ocean to the Arctic Ocean, it passes through the shallow eastern shelf of the Bering Sea which serves as a major sink of inorganic nitrogen. This study explores the physical and biological factors that influence the spatiotemporal variability of this sink. A regional relationship of dissolved inorganic nitrogen to inorganic phosphorus (DIN:P) was established for waters entering the shelf. Residuals from this relationship (termed N**) are a measure of the nitrogen deficit and were determined for bottom waters on the shelf using nutrient data collected on 52 hydrographic cruises spanning 2003 – 2018. Spatial variability in N** was related to advection, cross-shelf and vertical mixing, and residence time (using simulated ages of bottom water over the middle shelf). On average, this deficit accounted for approximately one-third of the inorganic nitrogen that enters the shelf, and the highest deficits (> 8 μM DIN) were observed on the middle shelf between 60°N and St. Lawrence Island (62°N). Temporal variability in N** was examined over the middle shelf, and higher nitrogen deficits that occurred in colder years were hypothesized to result from weaker flow and increased export of organic matter in the presence of sea ice. On the southern middle shelf, the volume integrated (40 m to bottom) seasonal change in N** was equivalent to a denitrification rate of 0.7 ± 0.3 mmol N m^{-2} d^{-1}. Rates of nitrogen loss were also estimated by combining N** with the simulated residence time of water on the shelf and found to be 0.20 ± 0.02 mmol N m^{-2} d^{-1}. These rates were comparable to prior measurements of denitrification/anammox reported on the shelf. The nitrogen deficit could not be wholly ascribed to denitrification/anammox as the N:P stoichiometric ratio in particulate matter is known to be lower at higher latitudes, and a lower ratio was observed when dissolved organic matter was measured in a small number of samples. It remains unclear how future reductions in sea ice might impact the extent of nitrogen loss in the Bering Sea.

25 Keywords

26 Bering Sea, Denitrification, Nitrogen Cycle, Nitrate, Ammonium, N**

1. Introduction

Primary producers (phytoplankton and algae) serve as the energy source for the marine environment through the conversion of nutrients and sunlight into a food base that ultimately sustains all marine life. In many marine environments, phytoplankton production is limited by nitrogen which is cycled in various forms (e.g., nitrogen gas [N_2], other forms of inorganic nitrogen, dissolved organic nitrogen) through the atmosphere, ocean, and sediments (Voss et al., 2013; Pajares and Ramos, 2019). Nitrogen fixation (conversion of N_2 into ammonia) and atmospheric deposition (Pearl et al., 2002; Kim et al., 2014) are the major sources of fixed nitrogen while production of N_2 through denitrification and anaerobic ammonium oxidation (anammox) are the primary sinks (Gruber and Galloway, 2008; Pajares and Ramos 2019). In the Bering Sea, the loss of inorganic nitrogen as N_2 is excessive and greatly alters the nutrient signature of water that flows from the North Pacific to the Arctic Ocean (Yamamoto-Kawai et al., 2006). Horak et al. (2013) found that 6.5 – 7.5 Tg yr^{-1} of fixed nitrogen is lost as N_2 through sedimentary processes (denitrification and/or anammox), an amount equivalent to ~16% of total nitrogen uptake by phytoplankton in the region. The majority of nitrogen loss (75 – 80%) occurs on the expansive eastern shelf of the Bering Sea rather than in the deep basin. These results were based upon direct measurements of the sedimentary N_2 flux and represented a 50% increase from prior estimates that were primarily based upon the sediment flux of dissolved inorganic nitrogen (DIN; nitrate + nitrite + ammonium) (Horak et al., 2013). The number of flux measurements, however, are too few to examine the spatiotemporal variability of nitrogen loss over the shelf.

The extent of fixed-nitrogen loss can be estimated from N*, which is the nitrate residual of the global nitrate:phosphate relationship, with negative values indicative of nitrogen loss (Gruber and Sarmiento, 1997; Deutsch et al., 2001; Deutsch and Weber, 2012). Utilizing this or

50 analogous parameters, large nitrogen deficits have been observed in bottom waters of the shelf
51 (Tanaka et al., 2004; Mordy et al., 2012; Granger et al., 2013; Horak et al., 2013) along with
52 unexplained seasonal and interannual differences in the nitrogen deficit reported between 2009
53 and 2010 (Horak et al., 2013).

54 Spatiotemporal variability of N* may result from changes in numerous factors, such as
55 the DIN:phosphate (hereafter DIN:P) signature in source waters that flow onto the shelf (e.g.
56 Bering Canyon versus Bering Slope Current) (Ladd, 2014; Stabeno et al., 2016); cross-shelf
57 exchange between source waters and the shelf (Stabeno and van Meurs, 1999; Mizobata et al.,
58 2006, 2008; Mordy et al., 2008, 2010; Sambrotto et al., 2008; Sullivan et al., 2008; Ladd et al.,
59 2012; Stabeno et al., 2016); unmeasured nitrogen pools (e.g. Dissolved Organic Nitrogen, DON)
60 that may erroneously be described as "missing nitrogen" and attributed to denitrification /
61 anammox; bottom temperatures, which thermo-regulate these benthic microbial processes;
62 residence time on the shelf during which the N* signal may accumulate (Stabeno et al., 2016);
63 export of organic matter (Moran et al., 2012) and its stoichiometric composition during export
64 and oxidation (Nedashkovskii et al., 2006; Martiny et al., 2013; Mills et al., 2015); and climate
65 factors that may be related to production and export, including wind mixing (Mordy et al., 2012;
66 Eisner et al., 2016; Liu et al., 2016) and ice coverage (Stabeno et al., 2012a; Sigler et al., 2014).
67 The goal of this paper is to examine the physical and biological processes that influence the
68 spatial and temporal (seasonal to interannual) variability of the nitrogen deficit on the eastern
69 Bering Sea (EBS) shelf.

70 In this paper, nutrient data from 52 hydrographic cruises spanning 2003 – 2018 (Table 1)
71 were used to explore the spatiotemporal variability of the nitrogen deficit on the EBS shelf.
72 Analogous to Codispoti et al. (2001) and Mordy et al. (2010), a regional DIN:P relationship was

established for waters entering the shelf, and a mixed model regression was used to determine the DIN residual in bottom water (termed N** to differentiate from N* that is based upon the global nitrate:phosphate relationship; Gruber and Sarmiento, 1997). The distribution of N** was mapped over the shelf, and spatial variability was related to advection, cross-shelf and vertical mixing, and residence time (using simulated ages of bottom water over the middle shelf). Temporal variability was examined over the middle shelf, and higher deficits corresponded to years with excessive sea ice and were hypothesized to result from changes in circulation and increased export of organic matter in the presence of sea ice.

2. Background

The EBS consists of a broad (> 500 km wide), shallow (< 180 m) shelf which is oceanographically partitioned into three domains; the inner (0 – 50 m bottom depth), middle (50 – 100 m) and outer (100 – 200 m) domains (Kinder and Schumacher, 1981a, b; Coachman, 1986; Kachel et al., 2002) (Fig. 1); and is further partitioned at ~ 60°N into the northern and southern shelves (Stabeno et al., 2012a). The primary source of water reaching the inner and the southern middle shelves is a combination of Gulf of Alaska water that enters primarily through Unimak Pass and slope water (Ladd et al., 2014; Stabeno et al., 2016). The slope water flows onto the shelf via Bering Canyon and its extension at the head of the canyon (Stabeno et al., 2016). In summer, northeastward flow through Bering Canyon is relatively weak and flow onto the shelf is primarily derived from Unimak Pass. In winter there is intensified northeastward flow through the canyon and flow onto the shelf is a mixture of waters from the Aleutian North Slope Current and the shallow eastern Aleutian Passes (primarily Unimak Pass; Ladd, 2014). Along the Alaska Peninsula, injection of nutrients from Bering Canyon supports high levels of new production (Kachel et al., 2002). The inner shelf from Bristol Bay to Nunivak Island has limited

replenishment, and the region is thought to be primarily a regenerative system (Granger et al., 2013; Mordy et al., 2017). The inner shelf is usually fully mixed (Kachel et al., 2002; Mordy et al., 2017), and northward flow is ~2 cm s^{-1} along the inner front (~ 50-m isobath) that separates the inner and middle shelves (Stabeno et al., 2016). In summer, this front largely restricts the influence of river discharge to the inner shelf.

The middle shelf is typically well-mixed in winter, and during winter, approximately 50% of the water on the southern middle shelf is replenished with slope water (Whitledge et al., 1986; Granger et al., 2013; Stabeno et al., 2016). There is considerable interannual variability in these estimates. Based upon wintertime salinities at the long-term mooring site M2 (56.9°N,

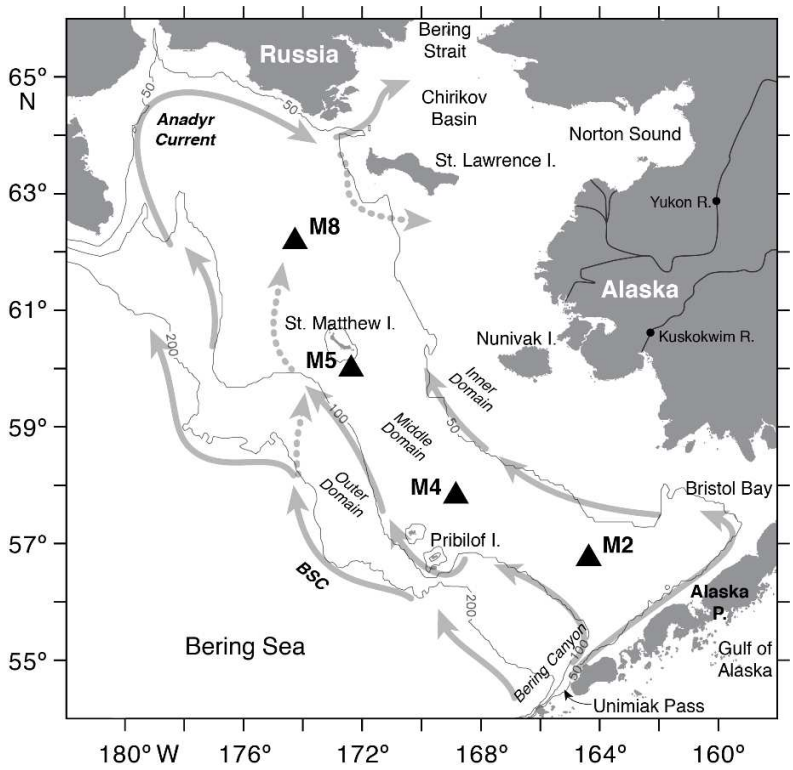

Figure 1. Map of the Bering Sea adapted from Stabeno et al. (2016) showing patterns of flow and long-term mooring sites (M2, M4, M5, M8). Gray arrows indicate patterns of flow and do not signify current speed. Dotted arrows signify intermittent flow. BSC is the Bering Slope Current.

164.1°W), 70 – 100% of water at M2 was replenished in 1999 and 2000, ~ 20% of water was replenished in 2010, and there was zero replenishment in 1997 (Stabeno et al., 2016). In summer, well-defined frontal structures (i.e., the inner front and the front between the middle and outer shelves) limit cross-shelf exchange on the southeastern shelf, except along the Alaska Peninsula.

The middle shelf in summer is defined by a two-layer system with a strong pycnocline separating a wind-mixed, nutrient-depleted surface layer from a tidally-mixed, nutrient-rich (5 – 10 μM nitrate) bottom layer (Stabeno et al., 2012a; Mordy et al., 2012). Remineralization of organic material in the bottom layer of the middle shelf results in summertime ammonium concentrations that are typically 4 – 8 μM (Mordy et al., 2008, 2010; Cheng et al., 2016) with a mid-depth ammonium tongue that extends over the outer shelf (Saino et al., 1983; Mordy et al., 2008). At the inner front, water can be entrained from the bottom layer of the middle shelf thereby introducing nutrients into the euphotic zone and supporting new production (Kachel et al., 2002; Mordy et al., 2017).

Averaged monthly flow on the middle shelf is generally weak (<1 cm s^{-1}), and the transit time from the M2 mooring to the northern shelf (~60°N) is a year or more (Stabeno et al., 2016). Hence, middle shelf waters are modified from one or more seasonal cycles of ice formation and retreat, winter advection (when the frontal structure has broken down) and mixing, and production and remineralization.

At the boundary between the middle and outer shelves, flow along the 100-m isobath is northward, but is weaker than the Bering Slope Current (BSC; Johnson et al., 2004; Johnson and Stabeno, 2017) with a transit time to Bering Strait of ~15 months (Stabeno et al., 2016). A number of processes foster exchange between the BSC and waters on the outer shelf including eddies, flow up canyons and interaction with other bathymetric irregularities (Stabeno and van

Meurs, 1999; Mizobata et al., 2006, 2008; Mordy et al., 2008, 2010; Sambrotto et al., 2008; Sullivan et al., 2008; Ladd et al., 2012; Stabeno et al., 2016). On the northern shelf, exchange between the outer and middle shelves occurs near the long-term moorings M5 and M8, and there is strong cross-shelf flow associated with the Anadyr Current (Fig. 1) (Coachman, 1975; Stabeno et al., 2016).

3. Methods

3.1 Hydrography

Data from several survey programs were combined to maximize spatial and temporal coverage of the shelf (Table 1). The National Oceanic and Atmospheric Administration (NOAA) Alaska Fisheries Science Center (AFSC) has conducted annual surveys in the Bering Sea in late summer to assess fish populations along a widely spaced (0.5° latitude x 1° longitude) sampling grid that encompasses the entire eastern shelf, although not all stations are sampled each year. These surveys include the Bering Arctic Subarctic Integrated Survey (BASIS), the Ecosystem Monitoring and Assessment (EMA) Program, and the Bureau of Ocean Energy Management (BOEM) funded Arctic Ecosystem Integrated Survey (EIS).

The NOAA's Ecosystems and Fisheries-Oceanography Coordinated Investigations (EcoFOCI; https://www.ecofoci.noaa.gov/) program conducts spring and late summer/early fall mooring cruises that usually incorporate hydrographic sampling along portions of the 70-m isobath. EcoFOCI has also completed several expansive hydrographic surveys, often in collaboration with larger programs (e.g. the Bering Sea Ecosystem Study [BEST]). During these surveys, most of these hydrographic transects had ~20-km station spacing to resolve physical and chemical gradients. Some cruises (e.g. AQ1301) only sampled a few stations during the transit south from Bering Strait.

151 During EcoFOCI cruises, conductivity-temperature-depth (CTD) measurements were
152 made with a Seabird SBE911[1] plus system with dual sensors for temperature and conductivity.
153 (Profiles of oxygen and chlorophyll fluorescence were also collected, but not used in this
154 analysis.) These sensors were calibrated by the manufacturer prior to the cruise. Data were
155 recorded during the downcast, with descent rates of 15 m min^{-1} to a depth of 35 m, and 30 m
156 min^{-1} below that. Salinity calibration samples were collected on most casts and analyzed on a
157 calibrated laboratory salinometer.
158 Discrete samples for nutrients were collected at 10-m depth intervals from the surface to
159 ~5 m off the bottom. Samples were collected from Niskin bottles and filtered through 0.45 µm
160 cellulose acetate filters. Samples were either frozen for later analysis at a shore-based facility
161 (typical for mooring cruises) or analyzed at sea (typical for major hydrographic surveys).
162 Dissolved inorganic nutrients (phosphate, silicic acid, nitrate, nitrite and ammonium) were
163 measured using automated continuous flow analysis with a segmented flow and colorimetric
164 detection. Standardization and analysis procedures specified by Gordon et al. (1994) were
165 closely followed including calibration of labware, preparation of primary and secondary
166 standards, and corrections for blanks and refractive index. Ammonium was measured using an

[1] Reference to trade names does not imply endorsement by NOAA

Table 1. Hydrographic cruises and the number of samples south of Bering Strait between 2003 and 2018 that are within 12 m of the bottom; include measurements of nitrate, nitrite, ammonium and phosphate; and have phosphate concentrations ≥ 0.5 µM. If multiple samples on a cast fit these criteria, only the deepest sample was included (i.e., there is only one sample per cast).

Year	Cruise ID	Ship	Dates	Samples	Year	Cruise ID	Ship	Dates	Samples
2003	BASIS - 2003	F/V Sea Storm	08/21 – 10/08	35	2011	DY1101	NOAAs Dyson	05/18 – 05/28	62
2004	HX288	R/V Alpha Helix	07/27 – 08/17	176	2011	MB1101	F/V Mystery Bay	08/15 – 09/10	9
2004	BASIS - 2004	F/V Sea Storm	08/16 – 09/28	69	2011	BASIS - 2011	NOAAs Dyson, F/V Bristol Explorer	08/21 – 09/23	110
2005	BASIS - 2005	F/V Sea Storm	08/16 – 10/05	43	2011	DY1104	NOAAs Dyson	09/22 – 09/27	24
2005	MF0513	NOAAs Freeman	09/22 – 09/28	61	2012	DY1204	NOAAs Dyson	04/29 – 05/08	21
2006	TN193	R/V Thompson	04/16 – 05/09	95	2012	AQ1201	F/V Aquilla	08/12 – 09/06	4
2006	BASIS - 2006	F/V Sea Storm, F/V NW Explorer	08/21 – 09/20	60	2012	BASIS - 2012	NOAAs Dyson, F/V Bristol Explorer	08/19 – 10/10	194
2006	MF0610B	NOAAs Freeman	09/26 – 10/05	76	2013	DY1305	NOAAs Dyson	05/03 – 05/10	52
2007	HLY0701	USCGC Healy	04/11 – 05/11	195	2013	AQ1301	F/V Aquilla	09/11 – 09/14	3
2007	BASIS - 2007	F/V Sea Storm, NOAAs Dyson	08/16 – 09/27	36	2013	BASIS - 2013	F/V Bristol Explorer	09/12 – 09/24	34
2007	TN211	R/V Thompson	09/27 – 10/09	103	2014	DY1405	NOAAs Dyson	05/07 – 05/17	86
2008	HLY0802	USCGC Healy	04/01 – 05/06	186	2014	DY1408	NOAAs Dyson	08/18 – 08/30	167
2008	HLY0803	USCGC Healy	07/04 – 07/30	170	2014	AQ1401L3	F/V Aquilla	10/15 – 10/19	4
2008	8M0823	R/V Melville	08/25 – 09/11	148	2015	DY1504	NOAAs Dyson	04/27 – 05/09	67
2008	BASIS - 2008	NOAAs Dyson	09/11 – 09/26	30	2015	DY1508	NOAAs Dyson	09/06 – 09/17	42
2009	HLY0902	USCGC Healy	04/05 – 05/11	188	2015	DY1509	NOAAs Dyson	09/24 – 09/30	70
2009	6N195J	R/V Knorr	06/14 – 07/12	185	2015	AQ1501	F/V Aquilla	09/24 – 09/24	1
2009	BASIS - 2009	NOAAs Dyson, F/V Epic Explorer	09/01 – 09/22	53	2016	DY1606	NOAAs Dyson	05/05 – 05/14	75
2009	MF0904L2	NOAAs Freeman	09/25 – 10/09	113	2016	DY1609	NOAAs Dyson	08/23 – 09/18	69
2010	PS1001	USCGC Polar Sea	03/13 – 04/05	78	2016	CF1601	F/V Cape Flattery	08/28 – 09/12	26
2010	DY1003	NOAAs Dyson	04/27 – 05/02	18	2016	DY1610	NOAAs Dyson	09/25 – 10/05	68
2010	TN249	R/V Thompson	05/11 – 06/13	166	2016	AQ1601	F/V Aquilla	09/27 – 09/29	3
2010	TN250	R/V Thompson	06/17 – 07/13	189	2017	DY1704	NOAAs Dyson	04/27 – 05/05	28
2010	BASIS - 2010	NOAAs Dyson, F/V Epic Explorer	08/18 – 10/08	132	2017	DY1708	NOAAs Dyson	09/23 – 10/04	49
2010	W1008B	R/V Wecoma	08/24 – 09/09	184	2018	DY1805	NOAAs Dyson	04/30 – 05/10	45
2010	MF1006	NOAAs Freeman	09/24 – 10/05	28	2018	AQ1801	F/V Aquilla	10/02 – 10/11	23

169 indophenol blue method modified from Mantoura and Woodward (1983). Standards were
170 prepared for each cruise, and there was frequent cross-comparison of primary and secondary
171 standards. Occasional comparisons were also made with commercial standards provided by
172 Ocean Scientific International Ltd (OSIL).

173 During BASIS cruises, CTD measurements were conducted primarily with a Seabird
174 SBE911plus, but a SBE25 served as a backup and was used on occasion. CTD sensors were
175 calibrated by the manufacturer prior to the cruise with additional salinity calibration samples
176 taken daily at one to two sample depths. From 2003 – 2011, discrete nutrient samples were only
177 collected at three to five depths, and in deeper water, the deepest sample was frequently > 12 m
178 off the bottom. Samples were stored frozen without filtration. Salinity and nutrient samples were
179 analyzed at a shore-based facility (University of Washington Marine Chemistry Laboratory).
180 Nutrient analysis followed colorimetric protocols set forth by Close et al. (1994) and were
181 comparable to methods used on the EcoFOCI cruise. Replicate frozen samples from the Bering
182 Sea were analyzed with each method and found to be within 0.5 µM nitrate, 0.04 µM nitrite, and
183 0.7 µM ammonium (SD, N = 13), and there was no significant difference between filtered and
184 unfiltered frozen samples (Mordy et al., 2010). Since 2012, BASIS and EcoFOCI cruises have
185 merged, and samples have been collected and processed according to the EcoFOCI protocols
186 including sampling depths, sample filtration and analysis.

187 In the summer of 2017, 71 samples were collected for analysis of total dissolved nitrogen
188 (TDN) and phosphorus (TDP). Results from this small subsample are presented at the end of the
189 manuscript to explore the influence of dissolved organic matter on the nitrogen deficit. These
190 samples were analyzed using the high temperature wet oxidation method of Valderrama (1981)
191 except for sample dilution. Prior to use, the potassium persulfate oxidant was recrystallized in

192 Milli-Q water to significantly reduce the nitrogen background. Each analytical run included a
193 dilution series of working standards prepared from stock solutions of potassium nitrate and
194 dibasic potassium phosphate, and oxidation efficiency standard solutions using a 15 µM nicotinic
195 acid standard for nitrogen and 1 µM glycerol-6-phosphate and 1 µM phosphonate for
196 phosphorus. Oxidized samples were analyzed for nitrate and phosphate content on a Seal
197 Analytical AA3 system using tubing configurations and flow rates specified by the manufacturer.
198 Each analytical run also included certified reference standard solutions (OSIL) for nitrate and
199 phosphate to confirm the accuracy of working standards. Compared to OSIL standards, working
200 standards yielded recoveries of 98% for nitrate and 102% for phosphate. Oxidation efficiency
201 standards yielded a recovery of 100% for nicotinic acid and 93-95% for glycerol-6-phosphate
202 and phosphonate.

203 *3.2 Determination of N***

204 The primary source of water (and nutrients) to the middle shelf of the Bering Sea is flow through
205 Unimak Pass and northeastward flow through Bering Canyon (Fig. 1) (Stabeno et al., 2016). To
206 derive a regional equation of N** for these source waters, a DIN:P relationship was determined
207 within and just north of Unimak Pass using data from 1111 samples taken at 138 stations that
208 were sampled between 2003 and 2016 (Figs. 2a, 2b). Stations west of Unimak Pass (Fig. 2a)
209 were not included in this analysis as some of this water turns north as part of the BSC (Ladd,
210 2014). In addition, some samples to the west of Unimak Pass had DIN residuals that were not
211 observed further east, perhaps due to substantial mixing as portions of water flow along or onto
212 the shelf (Mordy et al., 2005).

213 The sampling design included multiple measurements per station; therefore,
214 measurements among stations were not independent. Ignoring this sampling structure, any

hypothesis test would result in artificially inflating the degrees of freedom, making such tests invalid. Therefore, a random intercept mixed model was used based on restricted maximum likelihood (REML) that includes both fixed and random effects where "station" is treated as a random factor, thereby preserving the sampling structure. The linear mixed-effects (lme) function in the R Linear and Nonlinear Mixed Effects Models (nlme) package was used for analyses (R, ver. 3.3.2, Pinheiro et al., 2018). The residuals from the mixed model (based on Akaike Information Criteria [Akaike, 1973]) were determined for estimating the nitrogen deficit, or N** as:

$$N^{**} = DIN - (16.034^{*} PO_4^{-3}) + 6.914 + \varepsilon \quad (1)$$

where ε is the random effect to account for sample non-independence (0.5 ± 0.5 μM, mean ± SD).

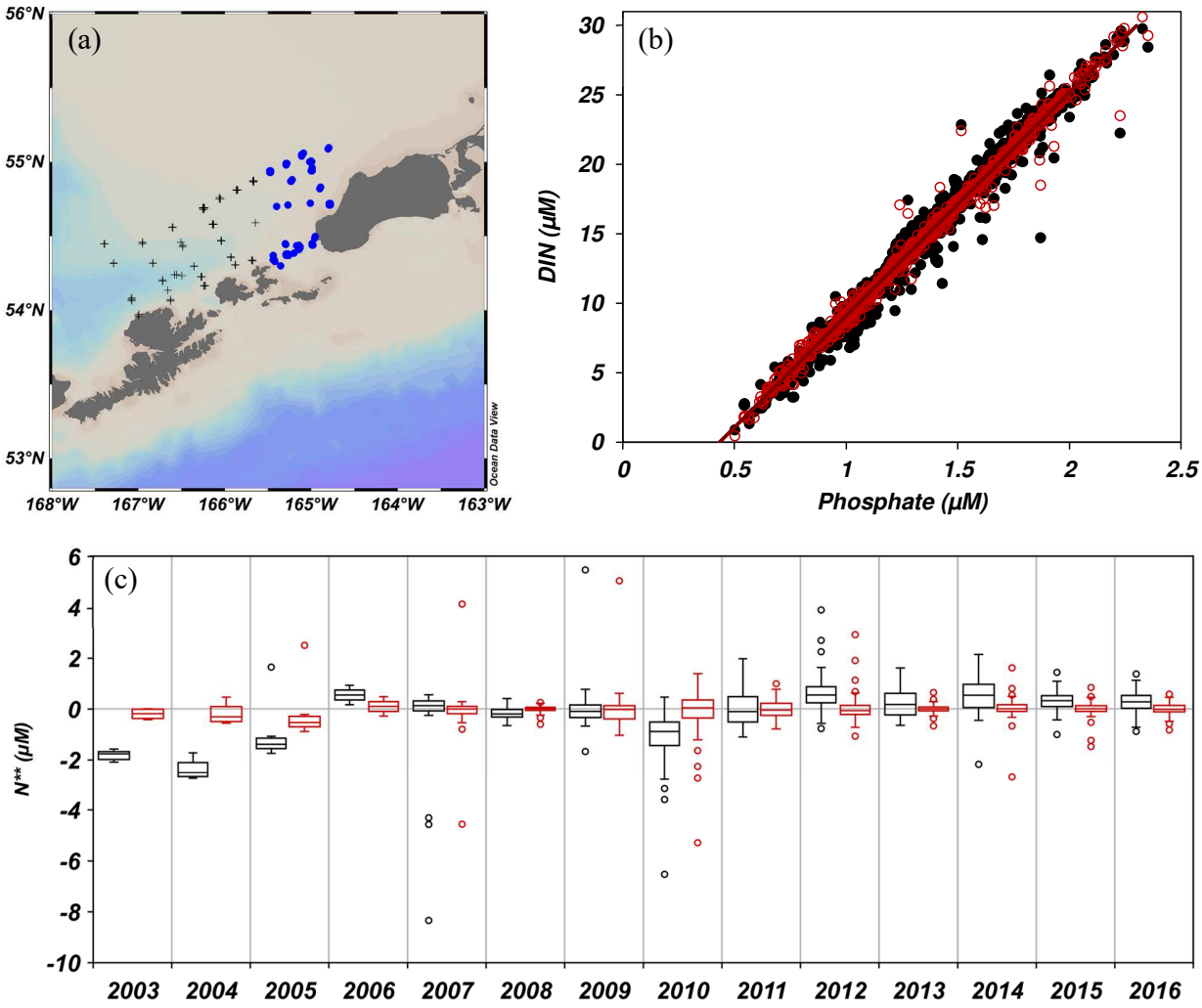

Figure 2. (a) The location of 144 stations (blue dots, some of which were frequently re-occupied) within and north of Unimak Pass that were used to determine the DIN:P relationship. Crosses are nearby stations not included in the analysis. (b) The DIN:P relationship in source waters of the southeastern Bering Sea shelf. Black dots are all data, and red circles are the residuals from the mixed model after accounting for sample non-independence (random effect). (c) Boxplots show the time series of N** (i.e. the residuals) from a simple linear regression (black) and from the mixed model (red) indicating the 1st (Q1) and 3rd (Q3) quartiles including the median value and "whiskers" indicating the minimum and maximum values that lie within 1.5 times interquartile range (Q3-Q1), and the circles indicate outliers.

227
228 *3.3 Spatiotemporal Variability of N***

To assess the spatiotemporal distribution of the nitrogen deficit, N** was determined on the deepest sample collected at each station with the following criteria: the sample was within 12 m of the bottom; sample analysis included nitrate, nitrite, ammonium and phosphate; and phosphate concentrations were ≥ 0.5 μM. The final data set includes 4153 stations with the majority of samples collected between 2007 and 2010 during the BEST program including 795 samples collected in 2010 (Table 1, Fig. S1). Spring sea ice has been a persistent feature of the northern middle shelf and limits the ability to sample early in the year in that region. During the BEST program, icebreakers USCGC *Healy* (2007 – 2009) and *Polar Star* (2010) were able to sample in the region despite icy conditions, and in recent years, reductions in ice cover has allowed more frequent sampling. Sampling was most frequent in September when the fall mooring cruise and the BASIS program generally occurred.

Seasonal variability was examined using 2292 samples over a narrow portion of the middle shelf (60 - 90 m bottom depth, excluding shallower samples near the Pribilof Islands, a region which behaves dynamically like the inner shelf). The data was partitioned into the northern (60°N to 63.3°N) and southern shelves (56°N to 60°N) (Stabeno et al., 2012a), and the data was divided seasonally into spring (March – May), summer (June – July), and fall (August – October).

3.4 Modeled Residence Times

To estimate the mean age of bottom water on the EBS shelf, an implementation of the Regional Ocean Modeling System (ROMS) was used. This is a free-surface, primitive equation hydrographic model (Shchepetkin & McWilliams, 2005; Haidvogel et al., 2008). The Bering Sea ROMS domain used in this study, hereafter referred to as the Bering10K model, spans the Bering Sea and northern Gulf of Alaska, with 10-km horizontal resolution and 30 terrain-following

252 depth levels (Hermann et al., 2013; Kearney et al., 2020). This domain is a subsection of the
253 larger Northeast Pacific (NEP5) domain (Danielson et al., 2011). Bathymetry derives from
254 ETOPO5, with smoothing for numerical stability and a minimum depth threshold of 10 m.
255 Mixing follows the algorithms of Large et al. (1994), with both ice (Budgell, 2005) and tidal
256 dynamics included. At the ocean-atmosphere boundary layer, bulk forcings relate winds, air
257 temperature, relative humidity, and downward shortwave and longwave radiation to surface
258 stress and net heat transfer (Large and Yeager, 2008).

259 For this analysis, an 18-year simulation of the Bering10K model was run beginning on
260 January 1, 2000 (initialized from a 1970-present hindcast). This period spans years of both high
261 sea-ice and low sea-ice extent, and therefore encompasses the typical interannual variability on
262 the EBS shelf. Surface forcings for our simulations were derived from historical reanalyses from
263 the Climate Forecast System (Saha et al. 2010). Boundary conditions for the open southern and
264 eastern boundaries use the hybrid radiation-nudging approach of Marchesiello et al. (2001), with
265 data from the Climate Forecast System reanalysis, while the northern boundary of the Bering10K
266 domain enforces a northward transport of 0.8 Sv through Bering Strait. Freshwater river runoff
267 was reconstructed from observed river discharge values (Kearney, 2019) and distributed as a
268 surface freshwater flux based on river mouth location with an e-folding scale of 20 km. Surface
269 salinities are restored to the monthly Polar Science Center Hydrographic Climatology (Steele et
270 al., 2001). Tidal harmonics were provided by the OTPS global tidal model (Egbert and Erofeeva,
271 2002). When coupled to this input dataset, the Bering10K model replicates observed interannual
272 variations in ice, bottom temperature, and other physical dynamics (Kearney et al., 2020).

273 The mean age of water calculation follows Zhang et al.'s (2010) implementation of
274 constituent-oriented age and residence-time theory. This method implements additional pairs of

tracers in the ROMS model; the first tracer in each pair is a conservative passive tracer (i.e. a dye tracer), while the second tracks an age concentration of the dye tracer. Mean age of the dye tracer can be calculated from the ratio between these two tracer variables. In our simulations, three pairs of dye tracers were added, each with a non-directional input flux of 5 units age-0 dye m^{-3} day^{-1} uniformly throughout the water column at a specified location. The first ~5 years of the simulation (2000 – 2005) represent a spin-up period, where the simulated mean age values on the eastern shelf accumulate over time. After this point, which corresponds to the maximum mean age of water on the shelf, drift in age values is minimal and variability reflects interannual variability in mixing and circulation.

Three distinct passive dye tracers were simulated to estimate aspects of the residence time of bottom water over the shelf (Fig. 3). All dye tracers were identical with the exception of their source locations: dye tracer 1 was released in Unimak Pass and Amukta Pass (52.4°N, 171.7°W); dye tracer 2 was released in every grid cell between 250 and 350 m bottom depth, i.e. along the continental slope ; and dye tracer 3 was released at the M2 mooring location. The first two tracers approximate the mean age of water since arriving on the shelf, either from the passes or from the shelf break. The third dye tracer provides an estimate of where water on the southeast middle shelf travels.

4. Results

*4.1 Determination of N***

In Eq. 1, the proportion of variance explained by the fixed effect in the mixed model, or the marginal R squared value was 0.97. The slope from this model was not significantly different than the Redfield (1958) N:P relationship of 16 (the 95% confidence interval [CI] of the mixed model was 15.92 – 16.15), however, the slope was significantly higher ($p < 0.001$) than the N:P

298 ratio observed over the outer shelf and along the continental slope of the Bering Sea (15.5;
299 Mordy et al., 2010).

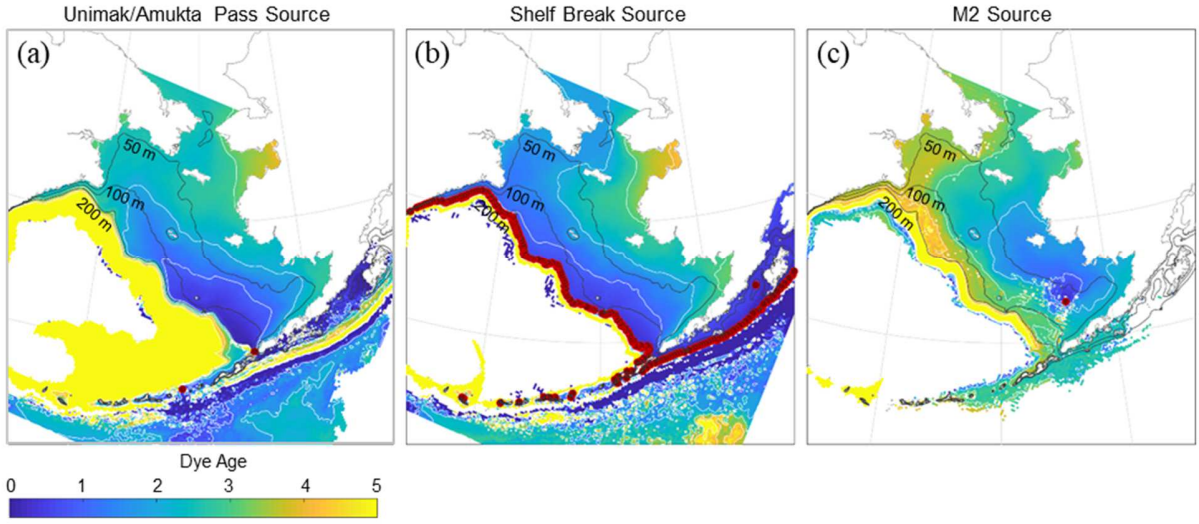

Figure 3. Simulated mean age of near-bottom water (temporally averaged over last 2 simulation years). Dye sources (red dots) uniformly emit a passive dye tracer through the water column (a) just north of Unimak Pass and Amukta Pass, (b) in every grid cell between 250 and 350 m bottom depth along the shelf break, and (c) at the M2 mooring. White contours are age in years, and dark gray contours are the 50, 100, and 200 m isobaths.

300 To test for a temporal trend in N** in source waters flowing northeastward through
301 Bering Canyon, the time series of N** near Unimak Pass was determined using a mixed model
302 and a simple linear regression. When calculated from the mixed model with station random
303 effects, there was no significant temporal trend between 2003 and 2016 ($p = 0.11$) (Fig. 2c, red).
304 Nor were there significant differences between annual means as the random effects partially
305 account for these. When a simple linear regression was applied (Fig. 2c, black), however, there
306 were significant differences in annual means (using Bonferroni correction), with the most
307 notable differences being that averaged means from 2003-2005 and 2010 (-1.5 ± 0.3, ± standard

error of the mean [SEM]) were significantly lower ($P < 0.0001$) than in 2006-2009 and 2011-2016 (0.2 ± 0.1 SEM). Systematic errors include the preparation of standards for each research cruise. Nitrate and phosphate standards typically vary by approximately 0.1 µM and 0.02 µM, respectively (unpublished data), and this translates into an additive error of ~ 0.4 µM in N** or, for example, ~ 50% of the median residual in 2010.

*4.2 Spatiotemporal Variability of N***

The relationship of DIN:P for all near-bottom samples is shown in Fig. 4a colored by latitude. Most of the samples were well below the Eq. 1 regression line indicating a nitrogen deficit relative to the Redfield ratio of water entering Bering Canyon. From Eq. 1, N** was determined for each sample and mapped over the eastern shelf (Fig. 4b). The largest deficits (> 8 µM DIN) were observed on the inner and middle shelf south of St. Lawrence Island and north of ~ 60°N. The smallest deficits were observed on the outer shelf and slope, north of St. Lawrence Island, and south of Nunivak Island. Temporal variability of N** was examined over the middle shelf. Tukey multiple comparison tests found that, on the southern middle shelf, spring, summer, and fall were all significantly different ($\alpha = 0.05$; Table 2, Fig. 5a). On the northern middle shelf, the nitrogen deficit was significantly different between spring and fall ($\alpha = 0.05$), but summer did not differ significantly from either spring or fall. To expand the early season data set, spring and summer data on the northern middle shelf were combined.

Seasonal and interannual variability of N** over the northern and southern middle shelf are shown in Table 3 and Figs. 5b and 5c. In both regions there were periods with small seasonal and interannual variability (e.g. 2008 – 2010), and other periods when the variability was relatively large (e.g. 2014 – 2018). On the southern middle shelf, the largest seasonal increases in the nitrogen deficit were observed in 2006 – 2007 and 2014 – 2018. For these years, the mean

331 seasonal (153 d) change in N** was -2.6 ± 1.1 µM N (± SD), which is equivalent to a
332 denitrification rate of 0.7 ± 0.3 mmol N m^{-2} d^{-1} when integrated over the bottom 40 m of the
333 water column, the typical thickness of the bottom layer on the middle shelf (Mordy et al., 2012;

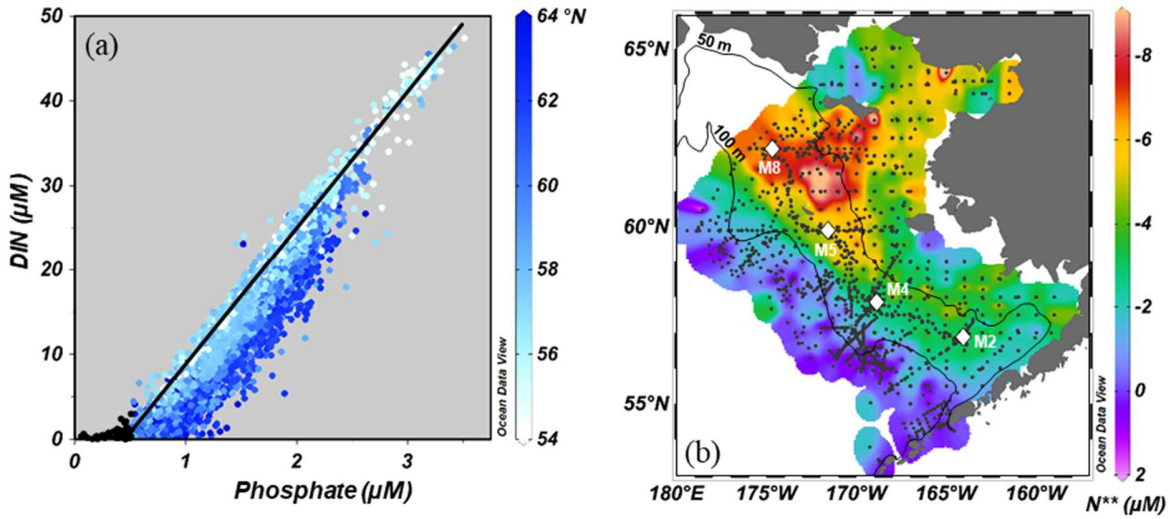

Figure 4. (a) The DIN:P relationship with data colored by latitude. The regression line is from Equation (1), and black dots indicate samples having < 0.5 µM phosphate that are not included in the analysis. (b) The distribution of N** for near-bottom samples in the eastern Bering Sea. The diamonds indicate the location of long-term mooring sites M2, M4, M5 and M8, and the black lines indicate the 50- and 100-m isobaths.

334

335 Table 2. Seasonal variability of N** in near-bottom samples over a narrow portion (60 – 90 m
336 bottom depth) of the northern (> 60°N) and southern (≤ 60°N) middle shelf [mean ± 95% CI
337 (number of samples)]. Data on the southern shelf is also shown for cold (2007-2010, 2012, 2013)
338 and warm (2003-2005, 2014-2016, 2018) years with the largest nitrogen deficits occurring in
339 cold years ($P < 0.0001$ in spring, $P = 0.02$ in fall). Spring is defined as March – May, summer is
340 June – July, and fall is August – October. Sample criteria are identical to Table 1.

Season	North N** (µM)	South N** (µM)	South Cold N** (µM)	South Warm N** (µM)

Spring	-5.9 ± 0.4 (133)	-2.6 ± 0.2 (578)	-3.0 ± 0.2 (310)	-1.3 ± 0.2 (145)
Summer	-6.2 ± 0.5 (108)	-3.6 ± 0.3 (250)		
Fall	-6.7 ± 0.3 (274)	-4.0 ± 0.2 (949)	-4.1 ± 0.2 (400)	-3.8 ± 0.2 (401)

341

342

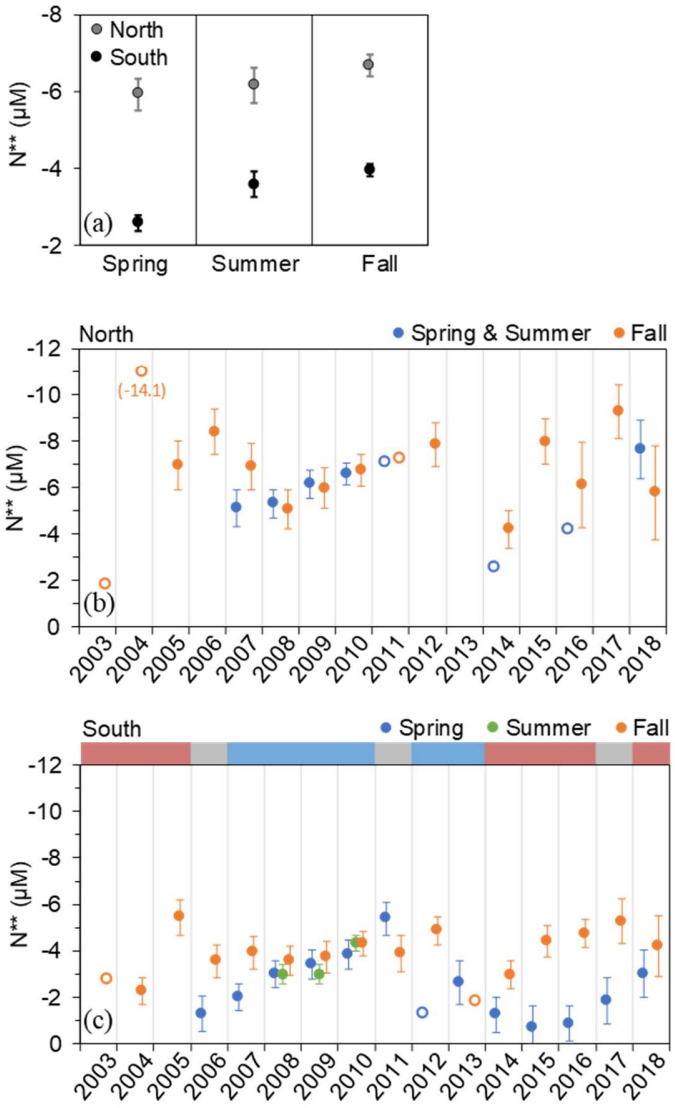

Figure 5. Seasonal trends (a) and interannual variability of N** on the northern (b) (> 60°N) and southern (c) middle shelf of the eastern Bering Sea. The colored bar above (c) indicates warm (red), cold (blue) or neutral (gray) conditions in the southern Bering Sea (Stabeno et al., 2012a, 2016; Stabeno and Bell, 2019). Error bars are the 95% CI. Open symbols indicate mean values with < 5 data points. Note that the y-axis shows increasing nitrogen deficit (more negative values). Spring is defined as March – May, summer is June – July, and fall is August – October. Sample criteria are identical to Table 1.

343

Table 3. Seasonal and interannual variability of N** in near-bottom samples on the northern and southern middle shelf [mean ± 95% CI (number of samples)]. Spring is defined as March – May, summer is June – July, and fall is August – October. Sample criteria are identical to Table 1.

Year	**North** Spring & Summer	**North** Fall	**South** Spring	**South** Summer	**South** Fall
2003		-1.9 (1)			-2.8 (1)
2004		-14.1 (1)			-2.3 ± 0.6 (97)
2005		-7.0 ± 1.0 (19)			-5.4 ± 0.8 (52)
2006		-8.4 ± 1.0 (22)	-1.3 ± 0.8 (45)		-3.6 ± 0.7 (62)
2007	-5.1 ± 0.8 (30)	-6.9 ± 1.0 (21)	-2.0 ± 0.6 (77)		-3.9 ± 0.7 (59)
2008	-5.3 ± 0.6 (52)	-5.1 ± 0.9 (28)	-3.0 ± 0.6 (72)	-3.0 ± 0.4 (66)	-3.6 ± 0.6 (79)
2009	-6.1 ± 0.6 (56)	-6.0 ± 0.9 (28)	-3.4 ± 0.6 (69)	-3.0 ± 0.4 (73)	-3.7 ± 0.7 (63)
2010	-6.6 ± 0.5 (83)	-6.7 ± 0.7 (48)	-3.8 ± 0.6 (63)	-4.3 ± 0.3 (111)	-4.3 ± 0.5 (106)
2011	-7.1 (3)	-7.3 (3)	-5.4 ± 0.7 (51)		-3.9 ± 0.8 (53)
2012		-7.8 ± 0.9 (24)	-1.3 (1)		-4.9 ± 0.6 (91)
2013			-2.6 ± 1.0 (28)		-1.9 (2)
2014	-2.6 (1)	-4.2 ± 0.8 (31)	-1.3 ± 0.8 (45)		-3.0 ± 0.6 (83)
2015		-8.0 ± 1.0 (22)	-0.7 ± 0.9 (30)		-4.4 ± 0.7 (69)
2016	-4.3 (4)	-6.1 ± 1.9 (6)	-0.9 ± 0.8 (46)		-4.7 ± 0.6 (81)
2017		-9.3 ± 1.2 (15)	-1.8 ± 1.0 (27)		-5.3 ± 1.0 (33)
2018	-7.7 ± 0.5 (12)	-5.8 ± 2.0 (5)	-3.0 ± 1.0 (24)		-4.2 ± 1.3 (18)

Stabeno et al., 2012a). In contrast, there was little seasonal change in other years, and in 2011 the nitrogen deficit on the southern middle shelf decreased from spring to fall. Interannual variability of N** in the northern and southern middle shelves were correlated in spring ($p = 0.02$) and fall ($p = 0.006$) (Fig. 6). This implies that factors influencing the nitrogen deficit are not confined to the biophysical boundaries that define the region (e.g. Stabeno et al., 2012a).

4.3 Modeled Residence Time

Patterns of dye dispersion generally reflect known patterns of flow (Kearney et al., 2020). Water from the passes flow northeastward through Bering Canyon towards M2 and into Bristol Bay, and flow northward along the 100-m isobath (Fig. 3a). Dye injected at the shelf break

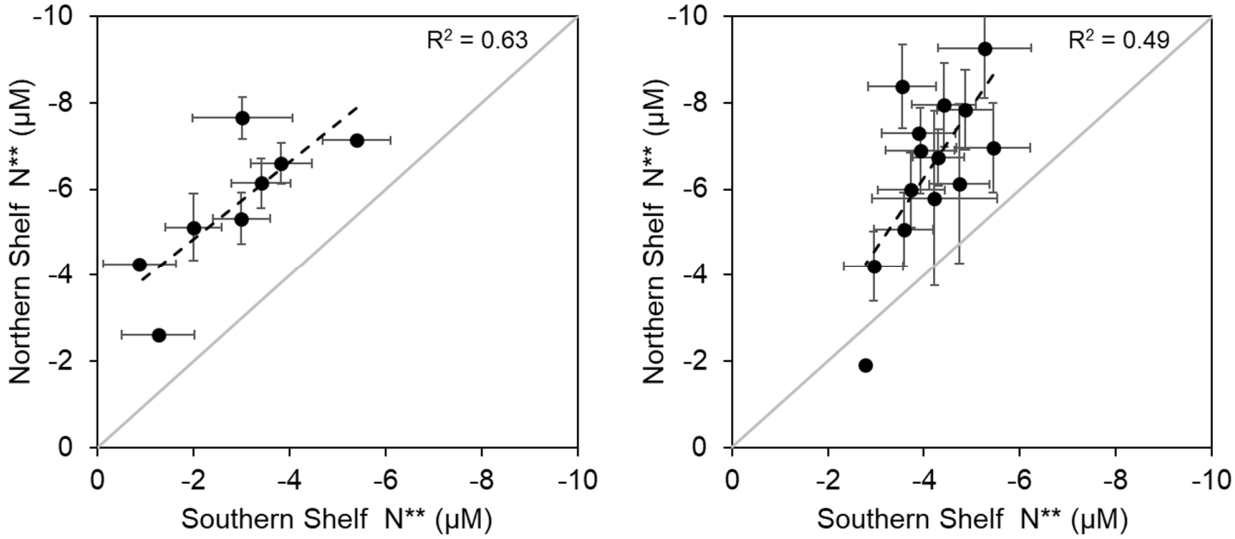

Figure 6. Relationship of N** between the northern and southern middle shelf of the eastern Bering Sea for individual years in spring (left) and fall (right). Note that the axes show increasing nitrogen deficit.

358

359

360 occupies the outer shelf and most of the middle shelf (Fig. 3b), and younger water north of St.
361 Lawrence Island is consistent with flow from the Anadyr Current. Modeled flow suggests that
362 the oldest water on the middle shelf occurs between St. Lawrence and St. Matthew Islands (Figs.
363 3a, b), consistent with the distribution of N** (Fig. 4b). On the southeastern shelf, the mean age
364 of water flowing north from M2 to the northern shelf (60°N) is two years (Fig. 3c). Patterns of
365 flow from M2 are weak and ill-defined, and while some water may transit to the northern shelf
366 within a year, water appears to recirculate in the northern region thereby increasing the mean
367 age.

To estimate a rate of nitrogen loss over the middle shelf, ages from the dye tracer 2 experiment (Fig. 3b) were assigned to each sample collected on a narrow portion of the middle shelf (60 – 90 m bottom depth, all latitudes) by aligning locations and sample date. Ages were unavailable for samples collected prior to January 1, 2006 and after December 31, 2017 (during spin-up and after the model simulation ends). When regressed with N**, there was a significant relationship ($F = 657$, $P < 0.0001$) with an estimated rate of nitrogen loss of 0.0050 ± 0.0004 mmol N m^{-3} d^{-1} (± 95% CI, N = 2062, Fig. 7).

5. Discussion

The EBS shelf is a significant sink of inorganic nitrogen for waters transiting between the North Pacific Ocean and the Arctic Ocean (Haines et al., 1981; Henriksen et al., 1993; Koike and Hattori, 1979; Tanaka et al., 2004). This results in a significant nitrogen deficit relative to the Redfield ratio that increases northward over the shelf and varies on seasonal and interannual time scales (Tanaka et al., 2004; Granger et al., 2013; Mordy et al., 2012; Horak et al., 2013). Herein, hydrographic data spanning 2003-2018 were used to further investigate processes influencing the spatiotemporal variability of the nitrogen deficit.

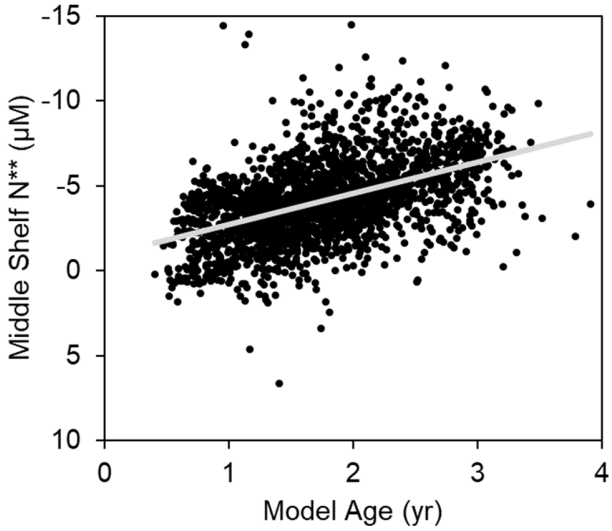

Figure 7. Linear regression of N** (µM) on modeled age of bottom water over a narrow portion of the middle shelf (60 – 90 m bottom depth). Note that the y-axis shows increasing nitrogen deficit.

*5.1 The influence of residence time on the distribution of N***

391 Negative values of N* are generally ascribed to the loss of inorganic nitrogen through
392 denitrification / anammox (Gruber and Sarmiento, 1997). On the EBS shelf, this is
393 predominantly a benthic process that modifies DIN:P ratios in the bottom mixed layer (Horak et
394 al., 2013). During BEST (2007 – 2010), denitrification rates across the eastern shelf of the
395 Bering Sea were obtained from direct measurements of the sedimentary N_2 flux and derived from
396 benthic respiration rates and the sedimentary flux of DIN (Horak et al., 2013). On average, the
397 denitrification rate in 2009 – 2010 was 1.0 ± 0.3 mmol N m^{-2} d^{-1} (± SEM, N = 27), and there was
398 no apparent latitudinal trend in denitrification rates between the northern and southern EBS shelf
399 (Supplemental Fig. S2). In the absence of a latitudinal trend in denitrification rates, spatial
400 variability in N** may simply be related to the residence time of water over the shelf.
401 The nitrogen deficit was smallest along the slope and outer shelf (Fig. 4b) where
402 northwestward mean currents are relatively strong (Fig. 1). Using several decades of satellite-
403 tracked drifter trajectories, Stabeno et al. (2016) estimated that the transit time along the 100-m
404 isobath from Bering Canyon to the northern shelf was ~8-9 months. Assuming a uniform
405 denitrification rate of 1.0 mmol N m^{-2} d^{-1}, a nitrogen deficit of ~ 6 µM would accumulate in a 40-
406 m bottom mixed layer along this path. The absence of this signal in Fig. 4b may be a
407 consequence of substantial mixing between the outer shelf and slope (discussed in Background).
408 Exchange between more denitrified water over the outer shelf with slope water may also explain
409 a slightly lower DIN:P ratio found along the slope (Mordy et al., 2012) than in Bering Canyon
410 (discussed in Results).
411 On the inner shelf, there is a latitudinal gradient in N** between Bristol Bay and Norton
412 Sound (Fig. 4b). The inner shelf is generally well mixed and there is stronger, well-defined flow
413 along the ~50-m isobath that is associated with the inner front (Kachel et al., 2002; Mordy et al.,

2017). These two processes reduce the residence time of bottom water on the inner shelf. The riverine influence on N** is uncertain as the nitrogen deficit was lower south of Nunivak Island, a region likely influenced by the Kuskokwim River, but not in the vicinity of the Yukon River. North of St. Lawrence Island, nutrient-rich Anadyr Water flows east into Chirikov Basin flushing this portion of the shelf with water from the outer shelf and slope (Coachman, 1975; Stabeno et al., 2017), thereby reducing the nitrogen deficit of waters flowing through Bering Strait and into the Chukchi Sea.

5.2 Estimating denitrification rates on the Middle Shelf

The latitudinal gradient in N** was greatest over the middle shelf, with the lowest N** values in the region between St. Lawrence Island, M5 and M8. North of 61°N, the nitrogen deficit on the middle shelf represents approximately one third (34 ± 9%, ± SD, N = 333) of inorganic nitrogen supplied through Bering Canyon (Fig. 8). This is comparable to results of Tanaka et al. (2004) who estimated that a third of nitrate entering the EBS shelf is lost through denitrification.

Transport over the middle shelf is weak with net flow being stronger in warm years (years with little or no ice; Stabeno et al., 2016). Model results suggest that net flow from M2 to M8 may take several years (Fig. 3c), which

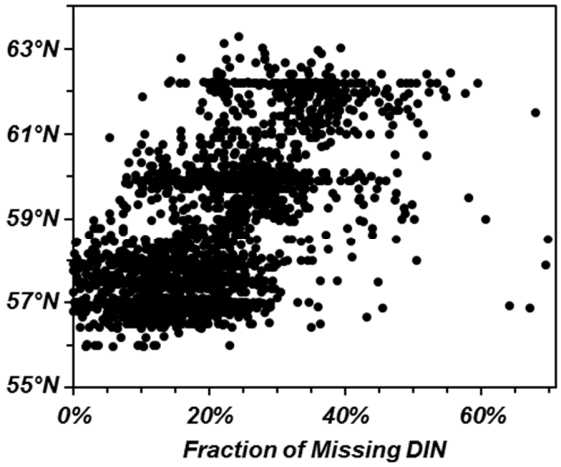

Figure 8. The fraction of missing inorganic nitrogen over a narrow portion of the middle shelf (60-90 m bottom depth) relative to a mean [DIN] of 20.8 µM from 334 near bottom samples collected over the middle shelf near Bering Canyon (55°-56°N, 163°-166°W, 50-100 m bottom depth).

is consistent with the results of Stabeno et al. (2016). Hence, during northward flow over the middle shelf the system will cycle through more than one summer where the two-layer system confines the N** signal to the bottom ~40 m of the water column (Horak et al., 2013). The system will also cycle through one winter where the water column is fully mixed, thereby reducing the residence time of the bottom water and evenly distributing the deep N** signal through the water column (see Figs. 4A and 5A in Horak et al., 2013). Strong winter winds can also result in strong cross shelf fluxes on the southeastern middle shelf that replenish the water column (Stabeno et al, 2016).

The Bering10K model simulates these seasonal processes and was used to estimate an age of bottom water corresponding to each N** sample from 2006 through 2017; the rate of nitrogen loss over the middle shelf was then calculated based on the resulting regression (Fig 7). Integrated over the bottom 40 m of the water column, the rate of nitrogen loss was 0.20 ± 0.02 mmol N m^2 d^{-1} (± 95% CI, N = 2062). Among the reported denitrification rates that are summarized in Table 5 of Horak et al. (2013), this rate is among the lowest, and is only ~20% of the mean denitrification rate. Model bias does not appear to be the primary source of this discrepancy as modeled flow along the 100-m isobath was consistent with drifter-derived estimates of flow (Stabeno et al., 2016; Kearney et al., 2020). Winter mixing of the bottom water N** signal through the water column is one process that could partially account for this low estimated rate of denitrification, and integrating over a 70 m water column provides a rate of 0.35 ± 0.03 mmol N m^2 d^{-1}.

*5.3 Spatiotemporal variability of N** on the Middle Shelf: Influence of circulation and ice*

The high degree of seasonal and interannual variability in N** (Fig. 5), and the correlation of variability over the northern and southern shelves (Fig. 6) indicates that physical

and/or biological factors that influence N** occur over relatively short time scales and large spatial scales. Two such factors include changes in circulation patterns that alter the residence time of water over the shelf, and the extent of ice coverage and concomitant export of organic matter. Both processes are forced by prevailing winds that alter the winter climate of the Bering Sea, and vary depending upon the position of the Aleutian low and corresponding storm tracks (Rodionov et al., 2007; Stabeno et al., 2016).

The seasonal cycle of the Bering Sea is defined by the presence or absence of sea ice (Stabeno et al., 2012a, 2012b). Sea-ice formation typically occurs on the northern shelf, and, with the prevailing northerly winds, polynyas generally occur south of all major islands (Kozo et al., 1990; Stabeno et al., 2012a) and sea ice is usually transported southward (Sullivan et al., 2014).

*5.3.1 Interannual variability of N** on the southeastern middle shelf: circulation and mixing*

While winter sea ice is a perennial feature on the northern shelf, ice is highly variable on the southeastern shelf with extensive ice in "cold" years due to persistent northerly winds that transport ice onto the southern shelf and little or no ice in "warm" years when periods of southerly winds limit the southern extent of sea ice (Sullivan et al., 2014; Stabeno et al., 2012b). Prior to 2000, there was high interannual variability between warm and cold years. Since 2000, there have been stanzas of warm (e.g., 2000–2005) and cold (e.g., 2007–2010) years interrupted by years with intermediate ice extent (Fig. 5) (Stabeno et al., 2012a, 2016, 2019).

During warm winters, periods of southerly winds result in net northward flow at the M2 and M4 moorings (see Fig. 14 in Stabeno et al., 2016). There is also evidence of on-shelf flow near the M5 mooring in warm years (Mordy et al., 2010; Stabeno et al., 2017). In contrast, during cold winters, the net surface flow at the M2 and M4 moorings is west-to-southwestward

and net bottom flow is weak (Stabeno et al., 2016). These different flow patterns are consistent with increased replenishment of shelf water during warm years and reflected in the model results showing simulated ages being younger in warm years (Fig. 9a). The weak but significant (P = 0.03) relationship between N** and modeled age suggests that interannual variability of N** in spring on the southern shelf may partially be related to variability in the residence time of the water over the shelf (Fig. 9a).

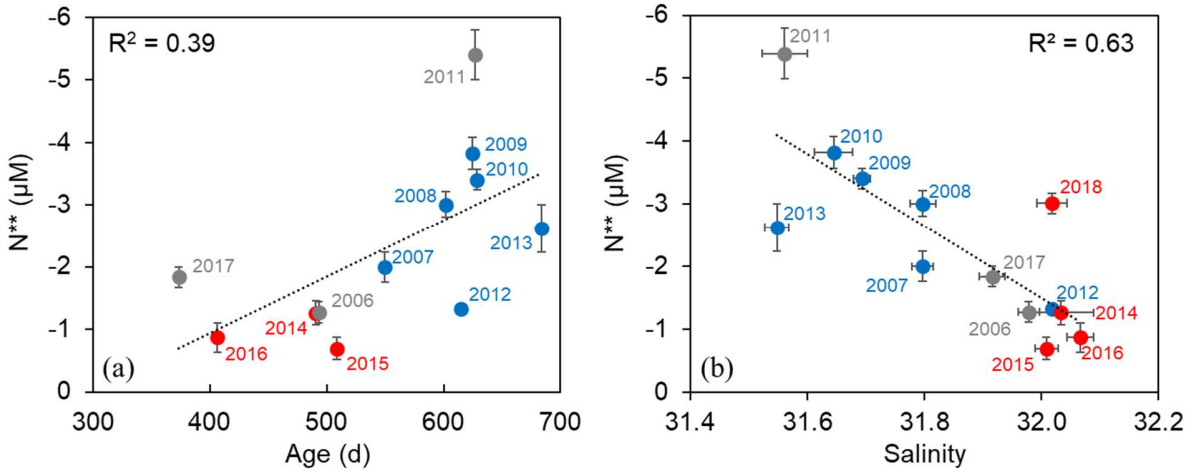

Figure 9. Linear regression of annual mean N** (μM) on the simulated age of water (a) and salinity (b) in spring (April-May) for bottom water over a narrow portion of the southern (≤ 60°N) middle shelf (60 – 90 m bottom depth). Colors represent warm (red), cold (blue) and transition (gray) years as in Fig. 5c. Note that the y-axis shows increasing nitrogen deficit.

Bottom salinities on the southeastern shelf also vary between warm and cold years (Fig. 9b). In warm years, stronger northward flow increases advection of higher salinity slope water that replenishes the middle shelf (Stabeno et al., 2016). In cold years, surface waters are freshened from a combination of ice melt and westward surface flow of fresher water near the inner shelf (Stabeno et al., 2016, Mordy et al., 2017). As ice retreat on the southern shelf

494 typically occurs prior to the cessation of storm mixing, surface freshening is often mixed through
495 the water column (Stabeno et al., 2012a).
496
497 *5.3.2 Interannual variability of N** on the southeastern middle shelf: Export production*
498 There was a significant (P = 0.001) relationship between N** and bottom salinities on the
499 southern shelf in spring with the largest nitrogen deficits occurring in cold years (Fig. 9b, Table
500 2). This finding implies that sea ice contributes to the seasonal and interannual variability of
501 N**. Sea ice exerts large impacts on the ecosystem (Stabeno et al., 2012a, 2012b, 2019) and
502 influences export production (Baumann et al., 2013). The biomass of ice algae in the Bering Sea
503 is among the highest reported in subarctic and Arctic regions, and its release during melting
504 promotes the rapid export of organic material to the benthos (Szymanski and Gradinger, 2016).
505 In a cold ice-covered spring, enhanced export of organic material to the benthos likely stimulates
506 early remineralization of nitrogen into inorganic and organic nitrogen pools and
507 denitrification/anammox (Fig. 9b).

508 Enhanced export of organic matter in cold years may also be promoted by secondary
509 producers. Zooplankton abundance is generally higher in cold stanzas (Hunt et al., 2011, 2016;
510 Stabeno et al., 2012b; Durbin and Casas, 2014; Coyle and Gibson, 2017; Ressler 2018, but see
511 Kimmel et al., 2018) and due to diel vertical migratory behavior (Schabetsberger et al., 2000)
512 zooplankton likely enhance the export of organic matter as fecal pellets directly to the benthos.
513 This hypothesis is supported by a significant relationship between N** and euphausiid
514 abundance (Fig. 10; P = 0.040 black, P = 0.026 green). While provocative, this relation may be
515 coincidence and requires further study.

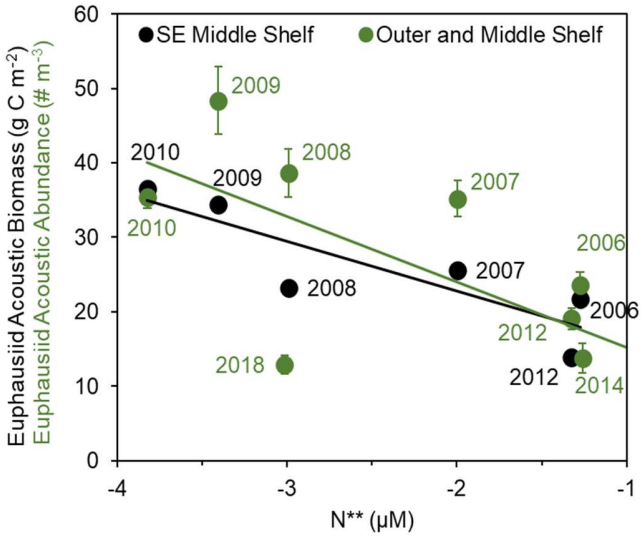

Figure 10. N** measured in spring on the southern middle shelf verses two summertime acoustic measurements of euphausiids: euphausiid biomass on the southeast middle domain spanning 2006-2012 (black; see Regions 3 and 6 in Table 2 of Hunt et al., 2016) and euphausiid abundance over the outer shelf and middle domains spanning 2006-2018 (green; Ressler, 2018).

516 Warm – cold differences in N** on the southern shelf are smaller in fall than in spring
517 (Table 2). On the southern shelf, if ice is absent (or retreats prior to mid-March), the spring
518 bloom is delayed until thermal stratification in May or early June (Sigler et al., 2014). While the

519 spring bloom may be delayed in warm years, overall primary production in warm years may be
520 enhanced relative to cold years (Brown et al., 2011; Brown and Arrigo, 2013; Lomas et al.,
521 accepted). If primary production is higher, but delayed in warm years, this may provide
522 extensive export production that occurs after the spring sample collection and could account for
523 more similar N** values between warm and cold years in fall.

524 *5.4 Variability of N** on the northern middle shelf*

525 As the northern middle shelf has been characterized by perennial winter ice, the warm –
526 cold designations used on the southern shelf generally do not apply. Similarity in spring and fall
527 N** from 2007-2011 might result if export production is dominated by ice algae, and
528 remineralization and denitrification/anammox is sustained prior to spring sampling (Fig. 5b).
529 Between 2014 and 2018, ice extent and conditions were highly variable with lowest winter ice
530 extent observed in 2018 (Stabeno and Bell, 2019; Stabeno et al., 2019), and these variable ice
531 conditions likely influence export production and may account for the high variability in N**
532 during these years (Fig. 5b). There was no trend in N** associated with variable ice conditions,
533 which precludes predictions on how the nitrogen deficit may be impacted by future warming.
534 Higher deficits on the northern middle shelf, however, will likely remain due to the longer
535 residence time of this water.

536 *5.5 Stoichiometry of dissolved organic nutrients*

537 It remains unclear if the nitrogen deficit represents nitrogen loss through denitrification /
538 anammox, pools of unmeasured nitrogen relative to phosphate (e.g. urea, other DON), or
539 variability in stoichiometric ratios of exported organic matter (Martiny et al., 2013). In the
540 summer of 2017, some additional samples were collected near Bering Canyon and along the 70-
541 m isobath at multiple depths for determination of total (inorganic and organic) dissolved nitrogen

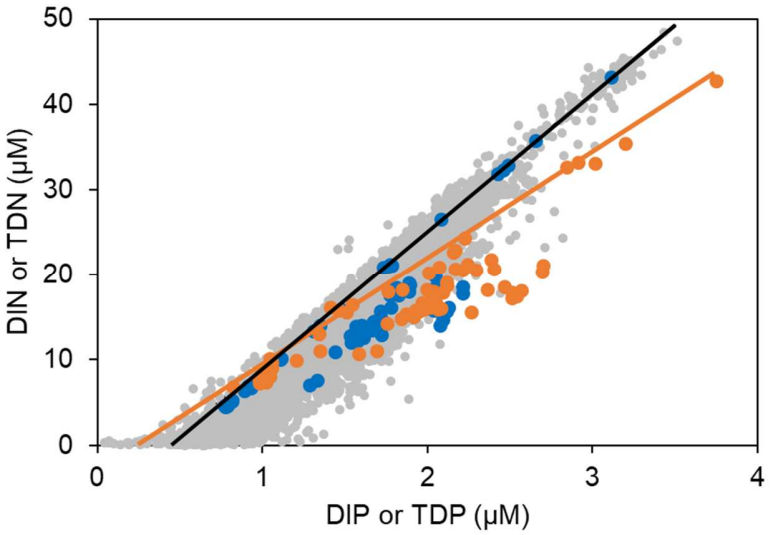

Figure 11. Relationship between DIN and DIP for all bottom samples over the shelf as in Fig. 1 (gray) overlaid with a subset of data from the summer of 2017 (cruise DY1708) with DIN versus dissolved inorganic phosphate (DIP) in blue and TDN versus TDP in orange. The black line is from Eq. 1, and the orange line represents an N:P ratio of 12.5 with an intercept of 0.26 µM phosphate.

(TDN) and phosphate (TDP) (Fig. 11). These findings imply that while inorganic nutrients reflect the Redfield ratio in Bering Canyon as in Eq. 1, the lower slope and intercept that results when including dissolved organic nutrients could reflect the lower N:P stoichiometric ratios of plankton observed at higher latitudes (Quigg et al., 2003; Martiny et al., 2013; Lomas et al., 2019; Schiffrine et al., 2020) that sink and remineralize in the benthos. Comparing N** calculated from a) Eq. 1 and dissolved inorganic nutrients versus b) the lower slope and total (inorganic + organic) dissolved nutrients, the nitrogen deficit in this subsample is reduced by ~10% when accounting for dissolved organic nutrients.

6. Summary

Extensive sampling during the past 15 years provides a unique view into the spatiotemporal variability of the bottom water nitrogen deficit (N**) on the EBS shelf. Spatially, the highest

553 deficits are observed on the middle shelf south of St. Lawrence Island, a region where net flow is
554 weak, residence time is high, there are frequent winter polynyas, and bottom waters are
555 seasonally isolated from surface waters. In this region the nitrogen deficit in bottom water
556 represents approximately one third of inorganic nitrogen that enters the shelf through Bering
557 Canyon. But these high deficits do not extend into Bering Strait due to onshelf flow of slope
558 water via the Anadyr Current. Rather bottom waters entering the Chukchi Sea have a moderate (-
559 3.9 ± 0.4 μM N [± SEM], N = 34) nitrogen deficit, and additional nitrogen loss occurs in the
560 Chukchi Sea as this region is also a significant nitrogen sink (Chang et al., 2009; Mills et al.,
561 2015). Temporally, seasonal and interannual variability in N** appears to be related to warm-
562 cold conditions on the shelf which influence circulation patterns and the export of organic
563 material (see Ward, 2013). While ice promotes the export of organic material in spring, in warm
564 years, primary production is delayed until the system begins to stratify, and productivity is higher
565 thereby increasing export production later in the spring and into the summer.

566 While distributions of N** are useful for examining the spatiotemporal distribution of the
567 nitrogen deficit over the shelf, this deficit cannot be fully ascribed to denitrification/anammox
568 (Mills et al., 2015). The derivation in this study (Eq. 1) is relative to inorganic nutrient ratios in
569 Barrow Canyon, and does not account for the assimilation, export and remineralization of
570 particulate matter at higher latitudes known to have lower N:P stochiometric ratios, or variability
571 in burial efficiency or in oxidation rates of organic nitrogen and phosphorus (Nedashkovskii et
572 al., 2006). Indeed, lower N:P ratios were found when considering both inorganic and organic
573 nutrient pools.

574 **Acknowledgements**

This is contribution No. 5089 for Pacific Marine Environmental Laboratory, contribution No. 2020-1072 for JISAO, and contribution No. EcoFOCI-0949 for NOAA's Ecosystem Fisheries Oceanography Coordinated Investigations. We thank the officers, captains and crew of the many vessels used to collect samples and data. We thank Bill Floering, Nancy Kachel, and David Kachel for assistance with field operations, and Sarah Battle for assistance with graphics, and Bonnie Chang and Sandra Bigley for comments that helped improve this manuscript.

Funding: This work was supported by the National Oceanic and Atmospheric Administration; the National Science Foundation, the Bureau of Ocean Energy Management CHAOZ, CHAOZ-X, and ArcWEST programs; and the Joint Institute for the Study of the Atmosphere and Ocean (JISAO) under NOAA Cooperative Agreement NA15OAR4320063.

586 **References**

587 Akaike, H., 1973. Information theory and an extension of the maximum likelihood principle. In
588 Petrov, B.N., Csaki, F. (Eds.), Second International Symposium on Information Theory
589 (Tsahkadsor, 1971) MR0483125, Akadémiai Kiadó, Budapest, pp. 267–281.
590 Baumann, M.S., Moran, S.B., Lomas, M.W., Kelly, R.P., Bell, D.W., 2013. Seasonal decoupling
591 of particulate organic carbon export and net primary production in relation to sea-ice at
592 the shelf break of the eastern Bering Sea: Implications for off-shelf carbon export.
593 Journal of Geophysical Research: Oceans 118(10), 5504–5522.
594 https://doi.org/10.1002/jgrc.20366
595 Brown, Z.W., Arrigo, K.R., 2013. Sea ice impacts on spring bloom dynamics and net primary
596 production in the Eastern Bering Sea. Journal of Geophysical Research: Oceans 118(1),
597 43–62. https://doi.org/10.1029/2012JC008034
598 Brown, Z.W., van Dijken, G.L., Arrigo, K.R., 2011. A reassessment of primary production and
599 environmental change in the Bering Sea. Journal of Geophysical Research: Oceans
600 116(C8), C08014. https://doi.org/10.1029/2010JC006766
601 Budgell, W.P., 2005. Numerical simulation of ice-ocean variability in the Barents Sea region.
602 Ocean Dynamics 55, 370–387.
603 Chang, B. X., & Devol, A. H. (2009). Seasonal and spatial patterns of sedimentary denitrification
604 rates in the Chukchi Sea. Deep Sea Research Part II: Topical Studies in Oceanography,
605 56(17), 1339-1350.
606 Cheng, W., Curchitser, E., Stock, C., Hermann, A., Cokelet, E., Mordy, C., Stabeno, P.,
607 Hervieux, G., Castruccio, F., 2016. What processes contribute to the spring and fall
608 bloom co-variability on the Eastern Bering Sea shelf?. Deep Sea Research Part II:

609 Topical Studies in Oceanography 134, 128–140.
610 https://doi.org/10.1016/j.dsr2.2015.07.009
611 Close, A.R., Knap, A.H. Michaels, A.F., 1994. Protocols for the Joint Global Ocean Flux Study
612 JGOFS core measurements. IOC SCOR UNESCO.
613 Coachman, L.K., 1986. Circulation, water masses, and fluxes on the southeastern Bering Sea
614 shelf. Continental Shelf Research 5(1-2), 23–108.
615 Coachman, L. K., Aagaard, K., & Tripp, R. B. (1975). Bering Strait: the regional physical
616 oceanography. University of Washington Press.
617 Codispoti, L.A., Brandes, J.A., Christensen, J.P., Devol, A.H., Naqvi, S.W.A., Paerl, H.W.,
618 Yoshinari, T., 2001. The oceanic fixed nitrogen and nitrous oxide budgets: moving
619 targets as we enter the anthropocene?. Scientia Marina 65(S2), 85–105.
620 Coyle, K. O., & Gibson, G. A. (2017). Calanus on the Bering Sea shelf: probable cause for
621 population declines during warm years. Journal of Plankton Research, 39(2), 257-270.
622 Danielson, S., Curchitser, E., Hedstrom, K., Weingartner, T., Stabeno, P., 2011. On ocean and
623 sea ice modes of variability in the Bering Sea. Journal of Geophysical Research: Oceans
624 116, 1–24.
625 Deutsch, C., Weber, T., 2012. Nutrient ratios as a tracer and driver of ocean biogeochemistry.
626 Annual Review of Marine Science 4, 113–141.
627 Deutsch, C., Gruber, N., Key, R.M., Sarmiento, J.L., Ganachaud, A., 2001. Denitrification and
628 N2 fixation in the Pacific Ocean. Global Biogeochemical Cycles 15(2), 483–506.
629 Durbin, E.G., Casas, M.C., 2014. Early reproduction by *Calanus glacialis* in the Northern Bering
630 Sea: the role of ice algae as revealed by molecular analysis. Journal of Plankton Research
631 36(2), 523–541. https://doi.org/10.1093/plankt/fbt121

632 Egbert, G.D., Erofeeva, S.Y., 2002. Efficient inverse modeling of barotropic ocean tides. Journal
633 of Atmospheric and Oceanic Technology 19, 183–204.
634 Eisner, L.B., Gann, J.C., Ladd, C., Cieciel, K.D., Mordy, C.W., 2016. Late summer/early fall
635 phytoplankton biomass (chlorophyll *a*) in the eastern Bering Sea: Spatial and temporal
636 variations and factors affecting chlorophyll *a* concentrations. Deep Sea Research Part II:
637 Topical Studies in Oceanography 134, 100–114.
638 https://doi.org/10.1016/j.dsr2.2015.07.012
639 Gordon, L.I., Jennings, J.C., Ross, A.A., Krest, J.M., 1994. A suggested protocol for continuous
640 flow analysis of seawater nutrients (phosphate, nitrate, nitrite, and silicic acid) in the
641 WOCE Hydrographic Program and the Joint Global Ocean Fluxes Study. WHP Office
642 Report 91(1).
643 Granger, J., Prokopenko, M.G., Mordy, C.W., Sigman, D.M., 2013. The proportion of
644 remineralized nitrate on the ice-covered eastern Bering Sea shelf evidenced from the
645 oxygen isotope ratio of nitrate, Global Biogeochemical Cycles 27(3), 962–971.
646 https://doi.org/10.1002/gbc.20075
647 Gruber, N., and Galloway, J. N., 2008. An Earth-system perspective of the global nitrogen cycle.
648 Nature, 451(7176), 293-296.
649 Gruber, N., Sarmiento, J.L., 1997. Global patterns of marine nitrogen fixation and denitrification.
650 Global Biogeochemical Cycles 11(2), 235–266.
651 Haidvogel, D.B., Arango, H., Budgell, W.P., Cornuelle, B.D., Curchitser, E., Di Lorenzo, E.,
652 Fennel, K., Geyer, W.R., Hermann, A.J., Lanerolle, L., Levin, J., McWilliams, J.C.,
653 Miller, A.J., Moore, A.M., Powell, T.M., Shchepetkin, A.F., Sherwood, C.R., Signell,
654 R.P., Warner, J.C., Wilkin, J., 2008. Ocean forecasting in terrain-following coordinates:

655 Formulation and skill assessment of the Regional Ocean Modeling System. Journal of
656 Computational Physics 227, 3595–3624.
657 Haines, J.R., Atlas, R.M., Griffiths, R.P. and Morita, R.Y., 1981. Denitrification and nitrogen
658 fixation in Alaskan continental shelf sediments. Appl. Environ. Microbiol., 41(2),
659 pp.412-421.
660 Henriksen, K., Blackburn, T.H., Lomstein, B.A. and McRoy, C.P., 1993. Rates of nitrification,
661 distribution of nitrifying bacteria and inorganic N fluxes in northern Bering-Chukchi
662 shelf sediments. Continental Shelf Research, 13(5-6), pp.629-651.
663 Hermann, A.J., Gibson, G.A., Bond, N.A., Curchitser, E.N., Hedstrom, K., Cheng, W., Wang,
664 M., Stabeno, P.J., Eisner, L., Cieciel, K.D., 2013. A multivariate analysis of observed and
665 modeled biophysical variability on the Bering Sea shelf: Multidecadal hindcasts (1970–
666 2009) and forecasts (2010–2040). Deep Sea Research Part II: Topical Studies in
667 Oceanography 94, 121–139. https://doi.org/10.1016/j.dsr2.2013.04.007
668 Horak, R.E.A., Whitney, H., Shull, D.H., Mordy, C.W., Devol, A.H., 2013. The role of
669 sediments on the Bering Sea shelf N cycle: insights from measurements of benthic
670 denitrification and benthic DIN fluxes. Deep Sea Research Part II: Topical Studies in
671 Oceanography 94, 95–105. https://doi.org/10.1016/j.dsr2.2013.03.014
672 Hunt, Jr., G.L., Coyle, K.O., Eisner, L.B., Farley, E.V., Heintz, R.A., Mueter, F., Napp, J.M.,
673 Overland, J., Ressler, P., Salo, S., Stabeno, P.J., 2011. Climate impacts on eastern Bering
674 Sea foodwebs: a synthesis of new data and an assessment of the Oscillating Control
675 Hypothesis. ICES Journal of Marine Science 68, 1230–1243.
676 https://doi.org/10.1093/icesjms/fsr036

677 Hunt, Jr, G.L., Ressler, P.H., Gibson, G.A., De Robertis, A., Aydin, K., Sigler, M.F., Ortiz, I.,
678 Lessard, E.J., Williams, B.C., Pinchuk, A., Buckley, T., 2016. Euphausiids in the eastern
679 Bering Sea: A synthesis of recent studies of euphausiid production, consumption and
680 population control. Deep Sea Research Part II: Topical Studies in Oceanography 134,
681 204–222. https://doi.org/10.1016/j.dsr2.2015.10.007
682 Johnson, G.C., Stabeno, P.J., 2017. Deep Bering Sea circulation and variability, 2001–2016,
683 from Argo data. Journal of Geophysical Research: Oceans 122(12), 9765–9779.
684 https://doi.org/10.1002/2017JC013425
685 Johnson, G, P. Stabeno and S. Riser, 2004.The Bering slope current system revisited. Journal of
686 Physical Oceanography 34 (2), 384-398.
687 Kachel, N.B., Hunt, Jr., G.L., Salo, S.A., Schumacher, J.D., Stabeno, P.J., Whitledge, T.E., 2002.
688 Characteristics and variability of the inner front of the southeastern Bering Sea. Deep Sea
689 Research Part II: Topical Studies in Oceanography 49(26), 5889–5909.
690 Kearney, K.A., 2019. Freshwater Input to the Bering Sea, 1950–2017. U.S. Dep. Commer.,
691 NOAA Tech. Memo. NMFS-AFSC-388, NTIS No. PB2019-100328, 46 pp.
692 Kearney, K., Hermann, A., Cheng, W., Ortiz, I., Aydin, K., 2020. A coupled pelagic-benthic-
693 sympagic biogeochemical model for the Bering Sea: documentation and validation of the
694 BESTNPZ model (v2019.08.23) within a high-resolution regional ocean model.
695 Geoscientific Model Development 13, 597–650. https://doi.org/10.5194/gmd-13-597-
696 2020
697 Kim, I. N., Lee, K., Gruber, N., Karl, D. M., Bullister, J. L., Yang, S., Kim, T. W., 2014.
698 Increasing anthropogenic nitrogen in the North Pacific Ocean. Science, 346(6213), 1102-
699 1106.

Kimmel, D.G., Eisner, L.B., Wilson, M.T., Duffy-Anderson, J.T., 2018. Copepod dynamics across warm and cold periods in the eastern Bering Sea: Implications for walleye pollock (*Gadus chalcogrammus*) and the Oscillating Control Hypothesis. Fisheries Oceanography 27(2), 143–158. https://doi.org/10.1111/fog.12241

Kinder, T.H., Schumacher, J.D., 1981a. Hydrographic structure over the continental shelf of the southeastern Bering Sea. In: Hood, D.W., Calder, J.A. (Eds.), The Eastern Bering Sea Shelf: Oceanography and Resources, vol. 1. NOAA Office of Marine Pollution Assessment, distributed by the University of Washington Press, Seattle, pp. 31–52.

Kinder, T.H., Schumacher, J.D., 1981b. Circulation over the continental shelf of the southeastern Bering Sea. In: Hood, D.W., Calder, J.A. (Eds.), The Eastern Bering Sea Shelf: Oceanography and Resources, vol. 1. NOAA Office of Marine Pollution Assessment, distributed by the University of Washington Press, Seattle, pp. 53–75.

Koike, I. and Hattori, A., 1979. Estimates of denitrification in sediments of the Bering Sea shelf. Deep Sea Research Part A. Oceanographic Research Papers, 26(4), pp.409-415.

Kozo, T.L., Farmer, L.D., Welsh, J.P., 1990. Wind-generated polynyas off the coasts of the Bering Sea islands. In: Sea Ice Properties and Processes: Proceedings of the WF Weeks Sea Ice Symposium, Monograph. US Army Corps of Engineers, pp. 90–91.

Ladd, C., 2014. Seasonal and interannual variability of the Bering Slope Current. Deep Sea Research Part II: Topical Studies in Oceanography 109, 5–13. https://doi.org/10.1016/j.dsr2.2013.12.005

Ladd, C., Stabeno, P.J., O'Hern, J.E., 2012. Observations of a Pribilof eddy. Deep Sea Research Part I: Oceanographic Research Papers 66, 67–76.

722 Large, W.G., Yeager, S.G., 2008. The global climatology of an interannually varying air–sea
723 flux data set. Climate Dynamics 33, 341–364.
724 Large, W.G., McWilliams, J.C., Doney, S.C., 1994. Oceanic vertical mixing: A review and a
725 model with a nonlocal boundary layer parameterization. Reviews of Geophysics 32, 363–
726 403.
727 Liu, C.L., Zhai, L., Zeeman, S.I., Eisner, L.B., Gann, J.C., Mordy, C.W., Moran, S.B., Lomas,
728 M.W., 2016. Seasonal and geographic variations in modeled primary production and
729 phytoplankton losses from the mixed layer between warm and cold years on the eastern
730 Bering Sea shelf. Deep Sea Research Part II: Topical Studies in Oceanography 134, 141–
731 156. https://doi.org/10.1016/j.dsr2.2016.07.008
732 Lomas, M.W., Baer, S.E., Acton, S., Krause, J.W., 2019. Pumped up by the cold: Elemental
733 quotas and stoichiometry of cold-water diatoms. Frontiers in Marine Science 6, 286.
734 https://doi.org/10.3389/fmars.2019.00286
735 Lomas, M.W., Eisner, L.B., Gann, J., Baer, S.E., Mordy, C.W., Stabeno, P.J., *Accepted for*
736 *publication*. Time-series of direct primary production and phytoplankton biomass in the
737 southeastern Bering Sea: Responses to cold and warm stanzas. Marine Ecology Progress
738 Series.
739 Mantoura, R.F.C., Woodward, E.M.S., 1983. Optimization of the indophenol blue method for the
740 automated determination of ammonia in estuarine waters. Estuarine, Coastal and Shelf
741 Science 17(2), 219–224.
742 Marchesiello, P., McWilliams, J.C., Shchepetkin, A., 2001. Open boundary conditions for long-
743 term integration of regional oceanic models. Ocean Modelling 3, 1–20.

744 Martiny, A.C., Pham, C.T., Primeau, F.W., Vrugt, J.A., Moore, J.K., Levin, S.A., Lomas, M.W.,
745 2013. Strong latitudinal patterns in the elemental ratios of marine plankton and organic
746 matter. Nature Geoscience 6(4), 279–283. https://doi.org/10.1038/ngeo1757
747 Mills, M.M., Brown, Z.W., Lowry, K.E., van Dijken, G.L., Becker, S., Pal, S., Benitez-Nelson,
748 C.R., Downer, M.M., Strong, A.L., Swift, J.H., Pickart, R.S., Arrigo, K.R., 2015. Impacts
749 of low phytoplankton NO_3^-:PO_4^{3-} utilization ratios over the Chukchi Shelf, Arctic
750 Ocean. Deep Sea Research Part II: Topical Studies in Oceanography 118, 105–121.
751 https://doi.org/10.1016/j.dsr2.2015.02.007
752 Mizobata, K., Wang, J., Saitoh, S.I., 2006. Eddy-induced cross-slope exchange maintaining
753 summer high productivity of the Bering Sea shelf break. Journal of Geophysical
754 Research: Oceans 111, C10017. https://doi.org/10.1029/2005JC003335
755 Mizobata, K., Saitoh, S.I., Wang, J., 2008. Interannual variability of summer biochemical
756 enhancement in relation to mesoscale eddies at the shelf break in the vicinity of the
757 Pribilof Islands, Bering Sea. Deep Sea Research Part II: Topical Studies in Oceanography
758 55(16), 1717–1728. https://doi.org/10.1016/j.dsr2.2008.03.002
759 Moran, S.B., Lomas, M.W., Kelly, R.P., Gradinger, R., Iken, K., Mathis, J.T., 2012. Seasonal
760 succession of net primary productivity, particulate organic carbon export, and autotrophic
761 community composition in the eastern Bering Sea. Deep Sea Research Part II: Topical
762 Studies in Oceanography 65, 84–97.
763 Mordy, C. W., Stabeno, P. J., Ladd, C., Zeeman, S., Wisegarver, D. P., Salo, S. A., & Hunt Jr, G.
764 L. (2005). Nutrients and primary production along the eastern Aleutian Island
765 Archipelago. Fisheries Oceanography, 14, 55-76.

766 Mordy, C.W., Stabeno, P.J., Righi, D., Menzia, F.A., 2008. Origins of the subsurface ammonium
767 maximum in the Southeast Bering Sea. Deep Sea Research Part II: Topical Studies in
768 Oceanography 55(16-17), 1738–1744.
769 Mordy, C.W., Eisner, L.B., Proctor, P., Stabeno, P., Devol, A.H., Shull, D.H., Napp, J.M.,
770 Whitledge, T., 2010. Temporary uncoupling of the marine nitrogen cycle: Accumulation
771 of nitrite on the Bering Sea shelf. Marine Chemistry 121(1), 157–166.
772 Mordy, C.W., Cokelet, E.D., Ladd, C., Menzia, F.A., Proctor, P., Stabeno, P.J., Wisegarver, E.,
773 2012. Net community production on the middle shelf of the eastern Bering Sea. Deep Sea
774 Research Part II: Topical Studies in Oceanography 65, 110–125.
775 Mordy, C.W., Devol, A., Eisner, L.B., Kachel, N., Ladd, C., Lomas, M.W., Proctor, P.,
776 Sambrotto, R.N., Shull, D.H., Stabeno, P.J., Wisegarver, E., 2017. Nutrient and
777 phytoplankton dynamics on the inner shelf of the eastern Bering Sea. Journal of
778 Geophysical Research: Oceans 122(3), 2422–2440.
779 https://doi.org/10.1002/2016JC012071
780 Nedashkovskii, A.P., Vanin, N.S., Khen, G.V., 2006. Spatial and temporal variability of the
781 ratios between the nitrate and phosphate concentrations in the Sea of Okhotsk.
782 Oceanology 46(3), 335–347.
783 Pajares, S., and Ramos, R., 2019. Processes and microorganisms involved in the marine nitrogen
784 cycle: knowledge and gaps. Frontiers in Marine Science, 6, 739.
785 Paerl, H. W., Dennis, R. L., Whitall, D. R., 2002. Atmospheric deposition of nitrogen:
786 implications for nutrient over-enrichment of coastal waters. Estuaries, 25(4), 677-693.

787 Pinheiro, J., Bates, D., DebRoy, S., Sarkar, D., R Core Team, 2018. nlme: Linear and Nonlinear
788 Mixed Effects Models. R package version 3.1-137, https://CRAN.R-
789 project.org/package=nlme.
790 Quigg, A., Finkel, Z.V., Irwin, A.J., Rosenthal, Y., Ho, T.-Y., Reinfelder, J.R., Schofield, O.,
791 Morel, F.M.M., Falkowski, P.G., 2003. The evolutionary inheritance of elemental
792 stoichiometry in marine phytoplankton. Nature 425(6955), 291–294.
793 Redfield, A.C., 1958. The biological control of chemical factors in the environment. American
794 Scientist 46, 205–221.
795 Ressler, P., 2018. Eastern Bering Sea Euphausiids ('Krill'). In: Siddon, E., & Zador, S.
796 Ecosystem Status Report 2018: Eastern Bering Sea, Stock Assessment and Fishery
797 Evaluation Report, North Pacific Fishery Management Council, Anchorage, AK, 99501,
798 pp. 88-90. https://access.afsc.noaa.gov/REFM/REEM/ecoweb/pdf/2018ecosysEBS-
799 508.pdf
800 Rodionov, S. N., Bond, N. A., Overland, J. E., 2007. The Aleutian Low, storm tracks, and winter
801 climate variability in the Bering Sea. Deep Sea Research Part II: Topical Studies in
802 Oceanography, 54(23-26), 2560-2577.
803 Saha, S., Moorthi, S., Pan, H.L., Wu, X., Wang, J., Nadiga, S., Tripp, P., Kistler, R., Woollen, J.,
804 Behringer, D., Liu, H., Stokes, D., Grumbine, R., Gayno, G., Wang, J., Hou, Y.T.,
805 Chuang, H.Y., Juang, H.M.H., Sela, J., Iredell, M., Treadon, R., Kleist, D., Van Delst, P.,
806 Keyser, D., Derber, J., Ek, M., Meng, J., Wei, H., Yang, R., Lord, S., Van Den Dool, H.,
807 Kumar, A., Wang, W., Long, C., Chelliah, M., Xue, Y., Huang, B., Schemm, J.K.,
808 Ebisuzaki, W., Lin, R., Xie, P., Chen, M., Zhou, S., Higgins, W., Zou, C.Z., Liu, Q.,
809 Chen, Y., Han, Y., Cucurull, L., Reynolds, R.W., Rutledge, G., Goldberg, M., 2010. The

NCEP climate forecast system reanalysis. Bulletin of the American Meteorological Society 91, 1015–1057.

Saino, T., Otobe, H., Wada, E., Hattori, A., 1983. Subsurface ammonium maximum in the northern North Pacific and the Bering Sea in summer. Deep Sea Research Part A. Oceanographic Research Papers, 30(11), 1157-1171.

Sambrotto, R.N., Mordy, C., Zeeman, S.I., Stabeno, P.J., Macklin, S.A., 2008. Physical forcing and nutrient conditions associated with patterns of Chl *a* and phytoplankton productivity in the southeastern Bering Sea during summer. Deep Sea Research Part II: Topical Studies in Oceanography 55(16-17), 1745–1760.

Schiffrine, N., Tremblay, J.É., Babin, M., 2020. Growth and elemental stoichiometry of the ecologically-relevant Arctic Diatom *Chaetoceros gelidus*: a mix of polar and temperate. Frontiers in Marine Science 6, 790.

Schabetsberger, R., Brodeur, R.D., Ciannelli, L., Napp, J.M., Swartzman, G.L., 2000. Diel vertical migration and interaction of zooplankton and juvenile walleye pollock (*Theragra chalcogramma*) at a frontal region near the Pribilof Islands, Bering Sea. ICES Journal of Marine Science 57(4), 1283–1295.

Shchepetkin, A.F., McWilliams, J.C., 2005. The regional oceanic modeling system (ROMS): A split-explicit, free-surface, topography-following-coordinate oceanic model. Ocean Modelling 9, 347–404.

Sigler, M.F., Stabeno, P.J., Eisner, L.B., Napp, J.M., Mueter, F.J., 2014. Spring and fall phytoplankton blooms in a productive subarctic ecosystem, the eastern Bering Sea, during 1995–2011. Deep Sea Research Part II: Topical Studies in Oceanography, 109, 71–83. https://doi.org/10.1016/j.dsr2.2013.12.007

833 Stabeno, P.J., Bell, S.W., 2019. Extreme conditions in the Bering Sea (2017–2018): Record-
834 breaking low sea-ice extent. Geophysical Research Letters 46(15), 8952–8959.
835 https://doi.org/10.1029/2019GL083816
836 Stabeno, P.J., van Meurs, P., 1999. Evidence of episodic on-shelf flow in the southeastern Bering
837 Sea. Journal of Geophysical Research: Oceans 104(C12), 29715–29720.
838 Stabeno, P.J., Farley, E., Kachel, N., Moore, S., Mordy, C., Napp, J.M., Overland, J.E., Pinchuk,
839 A.I., Sigler, M.F., 2012a. A comparison of the physics of the northern and southern
840 shelves of the eastern Bering Sea and some implications for the ecosystem. Deep Sea
841 Research Part II: Topical Studies in Oceanography 65–70, 14–30.
842 https://doi.org/10.1016/j.dsr2.2012.02.019
843 Stabeno, P.J., Kachel, N.B., Moore, S.E., Napp, J.M., Sigler, M., Yamaguchi, A., Zerbini, A.N.,
844 2012b. Comparison of warm and cold years on the southeastern Bering Sea shelf and
845 some implications for the ecosystem. Deep Sea Research Part II: Topical Studies in
846 Oceanography 65–70, 31–45. https://doi.org/10.1016/j.dsr2.2012.02.020
847 Stabeno, P.J., Danielson, S., Kachel, D., Kachel, N.B., Mordy, C.W., 2016. Currents and
848 transport on the eastern Bering Sea shelf: An integration of over 20 years of data. Deep
849 Sea Research Part II: Topical Studies in Oceanography 134, 13–29, Understanding
850 Ecosystem Processes in the Eastern Bering Sea IV.
851 https://doi.org/10.1016/j.dsr2.2016.05.010
852 Stabeno, P.J., Duffy-Anderson, J.T., Eisner, L.B., Farley, E.V., Heintz, R.A., Mordy, C.W.,
853 2017. Return of warm conditions in the southeastern Bering Sea: Physics to fluorescence.
854 PLoS ONE 12(9), e0185464. https://doi.org/10.1371/journal.pone.0185464

855 Stabeno, P.J., Bell, S.W., Bond, N.A., Kimmel, D.G., Mordy, C.W., Sullivan, M.E., 2019.
856 Distributed biological observatory region 1: physics, chemistry and plankton in the
857 northern Bering Sea. Deep Sea Research Part II: Topical Studies in Oceanography 162,
858 8–21. https://doi.org/10.1016/j.dsr2.2018.11.006
859 Steele, M., Morley, R., Ermold, W., 2001. PHC: A global ocean hydrography with a high-quality
860 Arctic Ocean. Journal of Climate 14, 2079–2087.
861 Sullivan, M. E., Kachel, N. B., Mordy, C. W., Salo, S. A., & Stabeno, P. J. (2014). Sea ice and
862 water column structure on the eastern Bering Sea shelf. Deep Sea Research Part II:
863 Topical Studies in Oceanography, 109, 39-56.
864 Sullivan, M.E., Kachel, N.B., Mordy, C.W., Stabeno, P.J., 2008. The Pribilof Islands:
865 temperature, salinity and nitrate during summer 2004. Deep Sea Research Part II: Topical
866 Studies in Oceanography 55(16-17), 1729–1737.
867 Szymanski, A., Gradinger, R., 2016. The diversity, abundance and fate of ice algae and
868 phytoplankton in the Bering Sea. Polar Biology 39(2), 309–325.
869 https://doi.org/10.1007/s00300-015-1783-z
870 Tanaka, T., Guo, L., Deal, C., Tanaka, N., Whitledge, T., Murata, A., 2004. N deficiency in a
871 well-oxygenated cold bottom water over the Bering Sea shelf: influence of sedimentary
872 denitrification. Continental Shelf Research 24(12), 1271–1283.
873 Valderrama, J.C., 1981. The simultaneous analysis of total nitrogen and total phosphorus in
874 natural waters. Marine Chemistry 10, 109–122.
875 Voss, M., Bange, H. W., Dippner, J. W., Middelburg, J. J., Montoya, J. P., Ward, B., 2013. The
876 marine nitrogen cycle: recent discoveries, uncertainties and the potential relevance of

877 climate change. Philosophical Transactions of the Royal Society B: Biological Sciences,
878 368(1621), 20130121.
879 Ward, B.B., 2013. How nitrogen is lost. Science 341(6144), 352–353.
880 https://doi.org/10.1126/science.1240314
881 Whitledge, T.E., Reeburgh, W.S., Walsh, J.J., 1986. Seasonal inorganic nitrogen distributions
882 and dynamics in the southeastern Bering Sea. Continental Shelf Research 5(1-2), 109–
883 132.
884 Yamamoto-Kawai, M., Carmack, E., McLaughlin, F., 2006. Nitrogen balance and Arctic
885 throughflow. Nature 443(7107), 43–43.
886 Zhang, W.G., Wilkin, J.L., Schofield, O.M.E., 2010. Simulation of water age and residence time
887 in New York Bight. Journal of Physical Oceanography 40, 965–982.